We responded to Referee #1 in the open discussion.

Response to Referee #2.

We thank the referee for the review, which contains interesting questions and comments. In the following, we answer each of them. We provide some further evidence that support the independence of our results on tuning of the applied methodology.

Reviewer: "a. PL detection and representation
1. How is the detection/tracking performed in ERA-5?" In the Rojo list, there are primary PL tracks, as well as secondary PL ones (in this case, there is usually no threshold on the associated surface wind speed, so that it is difficult to ensure that all are true PLs, according to the definition of Heinemann and Claud, 1987). Authors mention that they detect 243 of the 262 PL events of the list. In those 243 events, what is the proportion of primary PL which is detected? This might surely affect the results (see below)."

Response: Question 1: Matching of PLs from different datasets is challenging. It is a technical procedure that relies on subjective choices. The applied tracking and matching procedure is described in the manuscript. If demanded, we can provide further clarification on specific questions.
In order to give other scientists the possibility to test and reproduce our results, we provide the obtained PL list in the supplement. This list can be investigated if doubts remain on the quality of the applied detection. We add a sentence to the end of section 2.2 to make the reader more apparent about the supplement: "The list with the obtained PL tracks is provided in the supplement."
Additionally, we add: "We compared a random subset of obtained tracks with the PLs from the Rojo list, satellite imagery and ERA-5 fields, and concluded that vast majority of the obtained tracks can be considered to be PLs."

Question 2: The primary PL is detected for 242 of the 244 [1] PL events detected from the Rojo list. Note that in total 280 of the 374 PL centres (75%) are associated to a primary PL from the Rojo list, which means that in some instances several tracked PLs are associated to the same primary PL from the Rojo list. This can occur for example if a PL matches both with a primary and a non primary PL from the Rojo list. Additionally, one Rojo PL centre, since it has sometimes observational gaps of around 10 h, appears sometimes as two individual PLs in ERA-5. In turn 94 of the 374 PLs (25%) that we investigate are associated to a secondary PL from the Rojo list.

Reviewer: "A fair trajectory does not necessarily ensure that the PL is well represented, and in particular, surface wind speeds have been observed to be often

[1] In the last version of the manuscript this number was 243. One ERA-5 PL matches to two different Rojo events and one of these events was excluded in the previous version. However this excluded Rojo event has also an associated ERA-5 track, which appears reasonable by inspection of the system.

under-estimated in previous reanalyses, even after downscaling (e.g. Laffineur et al, 2014). Could the authors comment on this?"

Response: We agree that a track match does not ensure that the PL is well represented. We therefor add a sentence to the first paragraph of section 2.2: "Further, Stoll et al. [2020] demonstrated that the ECMWF model at comparable resolution as ERA-5 reproduced the 4 dimensional structure of one PL reasonably well."
We add at the end of the paragraph: "Note that this study does not rely on the completely realistic reproduction of every PL, as we mainly focus on the PL environment, which is well captured by ERA-5."
In total, we are confident that ERA-5 is reproducing PLs. For example the lifetime-maximum near-surface wind speed of 91% of the PLs from the list exceeds the threshold of 15 m/s, the common definition threshold for PLs (Fig. 1). For the remaining 9% of the systems ERA-5 may indeed underestimate the near-surface wind speed maximum.

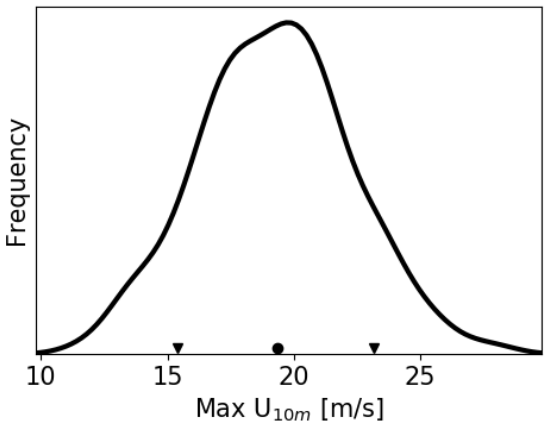

Figure 1: Frequency distribution of the 374 PLs in the lifetime-maximum area-maximum near-surface wind speed associated to the PL within a distance of 250 km from ERA-5. The distribution is estimated by a Gaussian kernel. The median, 10th and 90th percentile of the distributions are marked by a circle and triangles, respectively on the x-axis.

Reviewer: "3. Such methods usually detect more systems than in the reality. How many false positive PLs have been detected? Are they discarded ? In relation with the preceding point, the method of detection which has been selected is also questionable, Laffineur et al writing that 'caution is required with use of the 850-hPa vorticity, which may be indicative of troughs but not necessarily closed mesocyclonic circulations' "

Response: We do not agree with the interpretation that troughs are false positives. Heinemann and Claud [1997] and Rasmussen and Turner [2003] define PLs as mesoscale cyclones with some constraints. A trough is simply the superposition of a vortex (or cyclone) and the background flow. In our interpretation the PL definitions do not require that systems embedded in a strong background flow are

excluded from being PLs.
In summary, we are confident that the vast majority of the systems detected by our methodology can be classified as PLs. The near-surface wind speed distribution presented in Figure 1 provides further evidence.

Reviewer: "4. Is there a difference in the representation/detection of PL between the Norwegian and the Barents Sea, as noted by Smirnova and Golubkin, 2017?"

Response: Indeed there is a difference in accordance to Smirnova and Golubkin [2017]. We stated in line 104: "Hereby, 373 of the 420 PL centres from the Rojo list have at least one associated PL track." We remove this statement here since this comparison is done prior the exclusion due to lifetime and land. And insert the following later after line 113:
"In the Norwegian Sea 219 of 255 (86%) PL centres from the Rojo list are reproduced, whereas 129 of 165 (78%) are detected in the Barents Sea, where PLs in the Norwegian and Barents Sea are separated by the longitude of the first time step being smaller and larger than 20° E, respectively. A higher detection rate of STARS PLs for the Norwegian than the Barents Seas was also observed by Smirnova and Golubkin [2017]. It may be explained by STARS PLs being larger in the former than the latter ocean basin [Rojo et al., 2015] and larger systems being more likely captured by ERA-5."

Response to all points belonging to "a":
We have the impression that the reviewer indirectly asks for a sensitivity test of the robustness of the obtained results. In order to demonstrate the generality of the results, we repeat the SOM analysis on a set of systems that are with highest confidence to be classified as PLs. This set is a subset of the matched systems described in the manuscript with the following additional criteria:

- Match to a primary PL from the Rojo list. This means that systems matching only to secondary PLs from the Rojo list are excluded.

- A lifetime-maximum area-maximum near-surface wind speed that exceeds 20 m/s, in order to ensure that the PL is having an intensity considerably larger than the threshold of 15 m/s that is commonly applied as intensity threshold for PLs.

- A lifetime of matched PL tracks in ERA-5 of at least 12 h, to exclude short-lived systems that may not be well represented in ERA-5.

Of the 370 systems with 12,695 hourly time steps, the subset includes 113 PLs with 4,853 hourly time steps. The resultant SOM matrix based on the subset in the 850 hPa temperature anomaly (Figure 2) is similar to the SOM matrix based on the whole set (Figure 3 of Supplement). This demonstrates that the obtained results in the study are robust and not dependent on adaptations in the matching procedure. We therefore add an additional last sentence to section 2.2 of the manuscript: "The results of this study were found to be qualitatively insensitive to adaptations in the

track matching and exclusion."

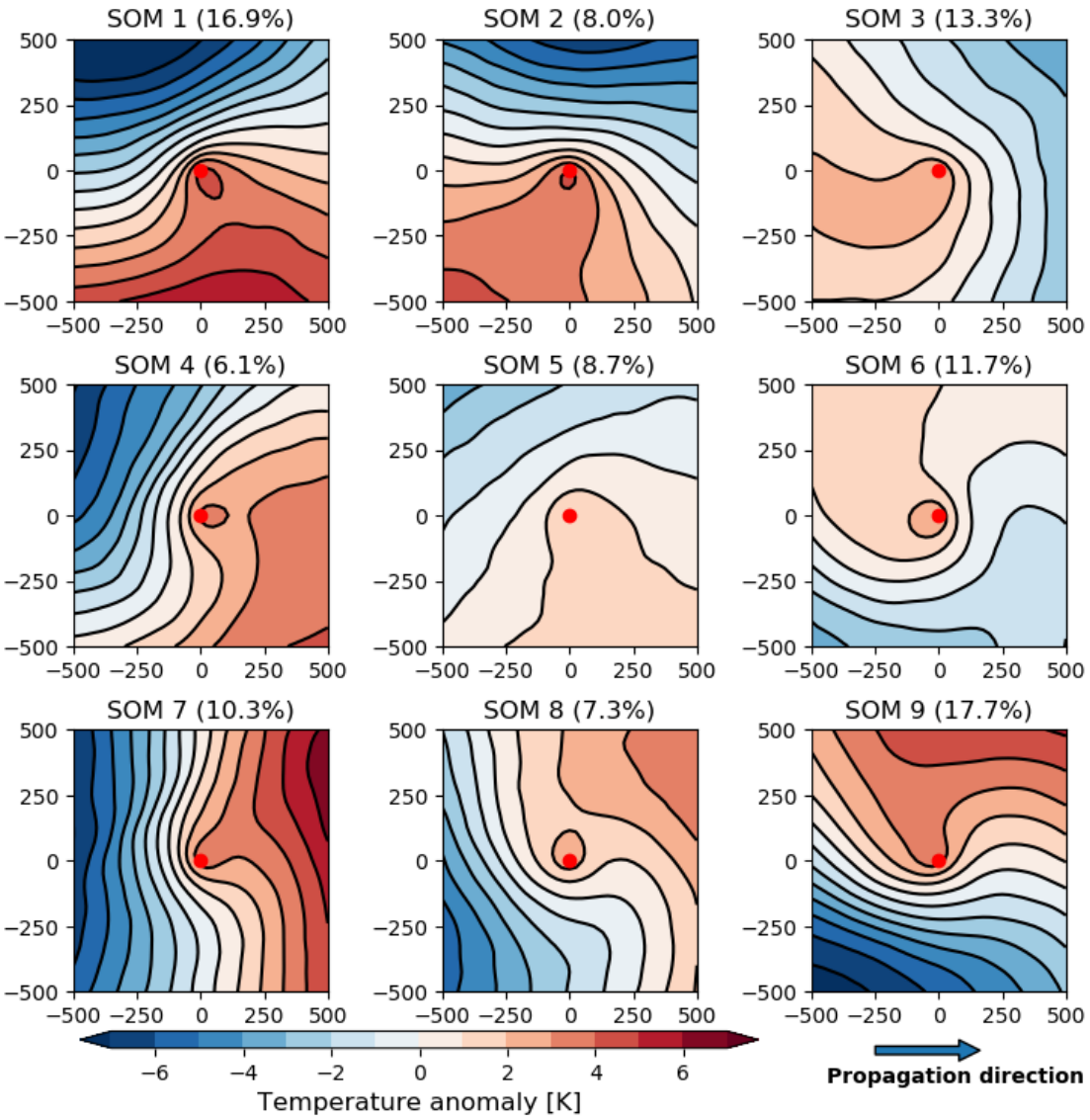

Figure 2: As Figure 3 of the Supplement, but based on the subset of 113 PLs with 4,853 time steps that satisfy additional criteria in order to test whether the results are robust.

Reviewer: "b. Regarding the use of the SOM method, there is a point that must be better justified: It seems to me that PL for which the shear situation changes during their lifetime (what is their proportion ?) should be discarded (I suspect that this would drastically reduce the size of the samples, which might be problematic). Otherwise this certainly affects the results and should prevent from drawing general conclusions. Also, would the results be modified if only primary PLs were used?"

Response: It is a result of our study that many PLs change their shear characteris-

tics during their lifetime, and not a weakness of the applied detection method. We further clarify this by formulating an additional paragraph at the end of Section 3.2:
"Note that this classification is based on individual PL time steps. In this way it is considered that the environmental shear often changes during the lifetime of an individual PL. The weak-shear class is the category with most time steps, however only 38 of the 374 PLs are within this class for their whole lifetime. In contrast, 189 PLs change between strong and weak shear during their development, mainly from strong to weak shear (Fig. 2). The shear angle varies by more than 90° during the lifetime for 80 of the 336 PLs that are featuring a strong shear. Hence, the shear strength and direction varies through the lifetime of an individual PL as its ambient environment changes."

Reviewer: "Concerning the interpretation of the results, one conclusion would be that there is no hurricane-like development. It might be the case in ERA-5, but this does not ensure that this is true in reality. This conclusion is too strong (at least based on the results presented here). On one side, they may not be (all) represented, and on the other hand, since these cases are probably seldom, it may well be that the method tends to smooth them. Is this method appropriate for cases that occur only occasionally?"

Response: We formulate the lack of hurricane-like PLs as an hypothesis drawn from the ERA-5 dataset. We suggest further investigation using a high-resolution dataset to test the hypothesis.

To the possibility that our methodology "smooths" hurricane-like PLs: We do not recognise outliers with hurricane-like dynamics within ERA-5 that are smoothed by our methodology. In Figure 5 of the manuscript, we present distributions in different variables and also display extreme values. We therefore formulate in the middle of section 3.3: "Moreover, extreme values in precipitation are lower for weak than for strong-shear situations (Fig. 5 dots), which contradicts the idea that convective processes are more important for the weak than the strong-shear class. Furthermore, the precipitation rates appear to be insufficient to represent intensification solely through convective processes, indicating that hurricane-like dynamics is unlikely in the weak-shear class."

Reviewer: "- last line of page 2 : "without an a-priori determination of a variable used for the categorisation". I don't understand this point. To me, the SOM method is applied on a single variable which has been choosen -T anomaly at 850 hPa- , it is not the algorithm which determines the variable(s) to be considered."

Response: We agree that this part of the sentence is misleading and therefore delete it.

Reviewer: "Rojo et al, 2019, JGR should be quoted. (see PANGAEA site)."

Response: We included the citation.

Response to Referee #3

We thank the third referee for the review, which contains interesting questions and comments. In the following, we answer to each of them.

Reviewer: "1. The detection method -The detection rate of the polar low depends on the thresholds used in the algorithm. Usually, weaker thresholds result in the higher detection rate, but they also cause more false detection. The false detection does not affect the polar low list in this study, because it is compiled by comparing the detected polar lows with "observed" polar lows in Rojo list. However, to evaluate the capability of ERA-5, the sensitivity to the threshold should be examined."

Response: Indeed, we could perform sensitivity tests, however an evaluation of ERA-5 is not the aim of this study. We reformulated the sentence in the abstract that specified a detection rate in ERA-5 in the previous version of the manuscript. We write in the end of Section 2.2: "Note that the detection rates depend on the applied matching criteria."

Reviewer: "-The authors use all timestep of detected polar lows. I think this means that polar lows with longer lifetime have larger effect on SOM analysis. Is that affects the result?"

Response: It is correct that polar lows with a longer lifetime have a larger effect on the analysis. We performed a SOM analysis just on the basis of initial (or mature) time steps and obtained similar SOM matrices, just with a different partitioning between the SOM nodes, or equivalently shear categories is slightly different. The weak-shear category was for example rather seldom if the SOM algorithm was applied on initial time steps only, which corresponds with results from our study (e.g. Fig. 5c). Hence, the result of the existence of different shear classes is general, but the fraction belonging to each of the shear situations is obtained on the time step level. It may well be that PLs persist in one shear situation for a longer time, a question that we did not investigate. However, a PL generally is not assigned to one shear category for the whole lifetime, which implies that partitioning into the shear categories on the system level instead of the time step level is challenging. We formulate a last paragraph to section 3.2 to make these points clearer:
"Note that this classification is based on individual PL time steps. In this way it is considered that the environmental shear often changes during the lifetime of an individual PL. The weak-shear class is the category with most time steps, however only 38 of the 374 PLs are within this class for their whole lifetime. In contrast, 189 PLs change between strong and weak shear during their development, mainly from strong to weak shear (Fig. 3). The shear angle varies by more than 90° during the lifetime for 80 of the 336 PLs that are featuring a strong shear. Hence, the shear strength and direction varies through the lifetime of an individual PL, because its

ambient environment may change. ”

Reviewer: ”2. Development mechanism of polar lows -The authors concluded that the orientation of the vertical-shear vector for the strong shear categories determines the dynamics of the systems. However, the fundamental development mechanism is moist baroclinic processes for all strong shear categories, while there are slight differences in their environments. Please clarify what is the different dynamics between these categories.”

Response: We agree that the previous formulation was misleading. Now, we formulate l.11: ”For the strong-shear categories, the shear vector organises the moist-baroclinic dynamics of the systems.”

Reviewer: ”-The authors mentioned the production of the potential vorticity associated with latent heat release. If this mechanism works, polar lows tend to move the direction of the maximum precipitation, which occurs in the warm sector. This is related to the diabatic Rossby vortex mechanism indicated by Terpstra et al. (2015). However, in Fig. 8, the distribution of the precipitation is not related to the propagation of the polar lows. Do the authors conclude the DRV mechanism does not account for the development of the polar low? Please clarify.”

Response: The mechanism that latent heat release can provide an additional source for low-level PV in a moist-baroclinic framework without the cyclone being classified as DRV [Davis and Emanuel, 1991; Stoelinga, 1996]. It appears indeed that the propagation of PLs is mainly determined by the mid-level wind (Fig. 3 of the manuscript). The location of the precipitation as compared to the centre of the PL, which varies for the shear situations (Fig. 8 of the manuscript), has limited influence on the propagation speed or direction of the PL. Hence as the reviewer notes, from a propagation argumentation it appears as if most PLs do not follow the DRV paradigm. Also the recognised (in a composite sense in Fig. 8) interaction of an upper and lower level perturbation (in a composite sense in Fig. 8) contradicts the DRV concept. However, even though the mean situations show a baroclinic interaction, this does not exclude that some PLs have DRV characteristics, a question we do not investigate.
However, we clarify the statement in section 4.2: ”The release of latent heat associated with the precipitation leads to the production of potential vorticity underneath the level of strongest heating and hence intensifies the low-level circulation within a moist-baroclinic framework [Balasubramanian and Yau, 1996; Davis and Emanuel, 1991; Kuo et al., 1991; Stoelinga, 1996].”
We further add a paragraph to the discussion and conclusion: ”The arrangement of the baroclinic structure in conjunction with the location of the latent heat release suggests a mutual interaction between the two. Latent heating enhances the baroclinicity and the diabatically-induced ascent is in phase with the baroclinically-forced adiabatic vertical motion. Thus, the effect of latent heat release is not only a linear addition to the dry-baroclinic dynamics, but also interacts directly with the adiabatic dynamics in a moist-baroclinic framework [Kuo et al., 1991].”

Reviewer: "L. 95: Why the authors used 850 hPa vorticity?"

Response: We considered it beneficial to use a level from the lower part of the troposphere, as the PL definition includes significant near-surface winds, however with a some distance from the surface in order to reduce influences from the boundary. Based on Figure 3 of Yanase et al. [2004], showing relatively uniform relative vorticity values for different levels in the lower troposphere, we do not expect that the choice of the level would make a considerable difference.

Reviewer:"L. 116: 13221 hourly time steps for 374 PL tracks means an average lifetime of 35.4 hour. This is almost upper end of the typical lifetime of the polar low (6-36h). Is this related to the higher capability of the ERA-5, i.e. the initial stage of the polar low can be detected?"

Response: Indeed, we guess that the lifetime estimates from observational datasets are likely biased towards lower values, as they are based on the time difference between the first and the last observation, whereas due to large time gaps between observations of sometimes multiple hours the precise genesis and lysis time likely occurs earlier and later, respectively. On the other hand, model based climatologies are likely biased towards longer lifetimes, as the simulation of larger and longer living systems is more accurate.

Reviewer:" L. 192: Is this mean that each PL has one time step for the mature stage and the timesteps before (after) the mature stage are categorized into genesis and lysis stage?"

Response: We define the genesis and lysis stages as the first and last time time step, respectively, of a given PL. We attempt to make this more clear now: "The PL time steps associated to genesis (intial), mature, and lysis (last) stages are counted for each node."

Reviewer:" L. 216 I think low-level trough is located slightly "down-shear" of the upper-level trough?"

Response: This is correct. Since we did not introduce the perspective with respect to the shear vector at this location in the manuscript, we change the formulation to downstream: "PLs in node 9 feature a low-level trough and a closed upper-level circulation slightly downstream." We provide the up-shear perspective in Section 4.1:

Reviewer:" Fig. 2: Do the amount of the transition include all timestep? If a polar low experience several transitions, are all transitions counted?"

Response: Indeed all transitions are counted, besides the back and forth transition as formulated in the end of section 2.5.: "Sometimes PLs transition back and forth between nodes, which indicates that the system is in a state between two nodes. We

disregard this back and forth development as it does not express a clear transition of the system."

Reviewer:" Fig. 4: I recommend the same arrangement of the number in the legend as the Fig. 2.?"

Response: A good comment. Due to a comment of the first reviewer, we removed the legend and added the numbers of the nodes to the figure.

Reviewer:" L. 345: Fig 7c -> Fig. 7d?"

Response: Thanks.

Reviewer:"L. 347: Fig 7d -> Fig. 7b.?"

Response: Thanks.

Reviewer:" L. 370-373: From this paragraph, I could not understand the updraft is associated with baroclinic (i.e. adiabatic) or diabatic process. Please clarify.?"

Response: True, this is not formulated very clearly. Here, we discuss the adiabatic process and we move the part of the low stability to the diabatic section. We now state: "Downstream of the upper-level trough the flow is diverging and hereby forcing mid-level ascent (Supplementary Fig. 11), which is co-located to the area of precipitation (second column in Fig. **??**). The rising motion occurs near the surface low pressure anomaly and further intensifies the PL through vortex stretching and tilting (not shown)."

Reviewer:"L. 434: Could you add the information about the number of transitions between shear category like Fig. 2.?"

Response: A good idea, we added an additional paragraph to the end of section 3.2: "The weak-shear class is the category with most time steps, however only 38 of the 374 PLs are within this class for their whole lifetime. In contrast, 189 PLs change between strong and weak shear during their development, mainly from strong to weak shear (Fig. 2 of the manuscript). The shear angle varies by more than 90°during the lifetime for 80 of the 336 PLs that are featuring a strong shear. Hence, the shear strength and direction varies through the lifetime of an individual PL, since its ambient environment may change."

Response to Referee #4

We thank the fourth referee for critical questions and feedback on the manuscript, which we think led to an improved manuscript. In the following we respond to each

of the points:

Reviewer: Major comment #1. Lines 138-139 – One may say that if PL radii vary from 150-600 km, in the case of small PL, you take a too large area around the vortex, which is not associated with its core. In the opposite situation, if the PL radius is 600 km, you cut the periphery, which is known to be the area of the maximum wind speed and turbulent fluxes. Depending on the addressed question, the area of 250 km around the PL center is too small (if you look at the largescale environment) or large (if you look at the processes inside the vortex itself). This might have a significant effect on the resulted composites. I would instead suggest using the estimate of PL radii presented in Rojo et al., 2015, and a buffer zone of a fixed size to cover all PL in the same way.

Response: We agree that there is some subjectivity in the choice of the 250 km radius to compute characteristics in different parameters associated to the PLs as displayed in Figure 5 of the manuscript. We therefore tested different radii for the different parameters and obtained qualitatively similar results. We added the sentence:" Presented results were found qualitatively insensitive to variations in the radius."
Calculating the parameter characteristics from the estimated radius from the Rojo list includes some challenges as well: 1. Most of the hourly time steps of the derived tracks do not have an associated Rojo track point, as the track points in the Rojo list have often time gaps of multiple hours. 2. The diameter from the cloud structure is also only a (subjective) estimate. 3. It causes problems when several PL centres are associated to one Rojo PL centre.

Reviewer: To provide the PL on the even grid, you can normalize them before the interpolation, like somewhat presented in Rudeva and Gulev, 2011 (Rudeva, I., and S.K. Gulev Composite analysis of the North Atlantic extratropical cyclones in NCEP/NCAR reanalysis. Mon. Wea. Rev., 139, 2011, 1419-1436.)

Response: This may be a good idea, but we consider the uncertainty in the scaling factor (i.e. size of the system) to be too large for performing such a normalisation. The emergent structures are clearly evident without such a scaling (Fig. 2) and it appears therefore not necessary.

Reviewer: Lines 155-157 – The same as for the previous comment. If you consider the mean wind vector in the area with a 500 km diameter around the PL center, in the case of large PLs (even 450 and 600 km in horizontal), you don't catch the environmental mean flow at all. My suggestion is to reconsider the area of the PL, at least as in the previous comment.

Response: It was written in line 157 that we use a radius of 500 km and not a diameter of this distance. We are confident that the mean wind vector within a distance of 500 km captures the environmental flow to a good approximation, as the influence of the PL vortex is filtered out by the mean. If the PL is to some de-

gree point symmetric this happens independently whether the PL is fully captured within the distance. Such symmetry would also be assumed if the PL is scaled. So, we do not see a benefit of variable distances. Again, we got similar results if we chose different radii.

Reviewer: Figure 8 – you never describe how you compute the composites since the simple mean for even a regular grid is not enough – all PLs have different sizes. Did you do the normalization by the PL diameter? Please, see Tilinina et al., 2018, for the description of what composites are.

Response: Indeed, we just calculate a simple mean of the time steps associated to the category. As mentioned earlier, a normalisation has also its caveats, and the main structures become apparent without normalisation. In fact, if the size of the system would really matter and contain different structures, these structures would be revealed by the SOM algorithm, at least in a large SOM matrix as shown in the Supplementary Figure 2. In other words, the SOM matrix would show a large and a small forward-shear node, if size would matter for forward-shear systems. But it does not and hence we conclude that the size is not of primary importance.

Reviewer: Major comment 2
Lines 226-227 Isn't it evident that baroclinic instability-induced vortices become thermally homogeneous at the lysis stage?

Response: Indeed. We did not write it here since baroclinic development is not discussed before these lines.

Wouldn't it be more correct to exclude lysis stages from the analysis of "archetypal meteorological conditions during the PL development" (line 62)?

Response: We interpret the development of PLs to also include the lysis stages.

Reviewer: Figure 2: 1. The evolution-transition blue arrows are messy and make the figure unreadable. 2. Again, the figure accounts for the same mesocyclones at different stages, which is quite confusing. I would rather plot the percentage of timesteps presented by each lifecycle stage in a particular node than the absolute value.

Response: Sure, Figure 2 includes a lot of information. We think that the depiction of absolute transition captures the information best, as the evolution can be followed. For example: Node 1: 62 PLs start in this node, 17+12+36 systems leave the node, 33+13 enter the node (+3 which are not displayed since the number is insignificant as denoted in the caption), hence 46 PLs end in this state. More PLs evolve from node 1 to 4 than in the opposite direction. It can be seen that node 1 is more common for genesis than lysis situation. However, node 5, which features most often lysis situation, has almost the same amount of lysis PLs. In summary, we think that most information is captured by using absolute values instead of frac-

tions.

Reviewer: Minor comments Line 33 – Talking about the hybrid nature of polar lows, I would suggest citing Terpstra et al., 2014.

Response: Do you mean the doctoral thesis from Terpstra?

Reviewer: Line 79 – It is better to say "ranges from 30 minutes up to 12 hours".

Response: Thanks

Reviewer: Line 90 – The tropopause is usually located at 300 hPa.

Response: The height stated here does not have any influence on the analysis. Anyway, we are more precise now in the formulation: "The reanalysis has 137 hybrid levels in the vertical, of which approximately 47 are below 400 hPa, which is the typical height of the tropopause in polar-low environments [Stoll et al., 2018]."

Reviewer: Lines 90-91 – 1. As far as I know, polar lows are not presented a lot poleward of 80N, so the problem of longitude convergence might not be a large one in the considered area. 2. How did you do the coarsening of data in a longitudinal direction? Did you calculate the mean of each two longitudinal points? Please, clarify it in the text.

Response: We do not state that longitude convergence is a problem, but we chose a coarser grid in the zonal direction to save space on our file system. At 60°latitude, a grid cell with equal lat/lon grid spacing would have a zonal length increment only half of the meridional increment. Hence, it makes more sense to use an unequal grid in the lat/lon space. However, it does not matter for our analysis, as we interpolate to a polar-low centred grid later.
The ECMWF model is spectral and the parameters are archived as spectral coefficients [2]. The requested fields are automatically converted and interpolated to a regular lat/lon grid, which the user has to define.

Reviewer: Line 117 – How did you associate the automatically detected by the vorticity field PLs with that detected in satellite data from the Rojo list? Please, clarify it in the text.

Response: We stated in line 104: "All tracks that have a distance of less than 150 km to a PL from the Rojo list for at least one time step are regarded as matches."

Reviewer: Line 135 – why don't you just extend the ERA-5 boundaries chosen for the analysis to cover the four excluded mesocyclones? Furthermore, how did you estimate the influence of this elimination?

[2]https://confluence.ecmwf.int/display/CKB/ERA5%3A+What+is+the+spatial+reference

Response: We could, but only less than 4% of the time steps that are excluded and it would require to download a considerable amount of additional data. We are confident that our results are robust that these excluded time steps would not change them.

Reviewer: Line 165 – from where the 60 rm radius filter came from? Does it have any physical meaning? Please, provide an argumentation for this choice in the text of the manuscript. Why not use the Savitzky-Golay filter only?

Response: It comes from line 99 and we specify this in the sentence of line 164. We now add a parenthesis after the sentence: "These maxima are based on the spatially-smoothed vorticity using a uniform filter of 60 km radius (point two of the algorithm modifications in Sec. 2.2)"
These spatially-filtered vorticity maxima are used to detect the PLs, as they identify locations of strong mesoscale vortexes. We think it is most consistent to use the same intensity measure as used for the identification of the systems.

Reviewer: Line 170 – "of a time step" instead of "of an time step."

Response: Thanks

Reviewer: Lines 192-193 – There is a more common practice to distinguish between different stages of the lifecycle of any cyclonic phenomena – normalizing the number of timesteps and letting 0-0.2 to be the genesis stage, 0.2 – 0.8 to mature stage, and 0.8 to 1 to lysis (see Simmonds, 2000; Rudeva and Gulev, 2007 for example). How can you prove your choice of the mature stage definition?

Response: We consider it logical to define the mature stage as the time step with highest intensity. As indicated in the response to "major point 2", by assigning only one time step per PL to each of these steps, individual PL transitions can be compared.

Reviewer: Lines 196-197 – The statements done on these lines need to be proven by some citation or description on why some signal may be simply removed from the analysis like these transition states of the system.

Response: The SOM method is a method of classifying data, where strict thresholds between the classes may not exist. Hence, if a PL is transitioning back and forth between two SOM nodes, the PL is apparently in a state between these classes, we do not think this needs any proof. Further, if we do not apply the removal of back and forth transitions the results would be similar (compare Fig. 3 to Figure 2 of the manuscript). More transitions are from strong shear to weak shear situations. However, many of the transitions from weak to strong shear are due to these back and forth transitions, hence we prefer the depiction of the manuscript.
Reviewer: Line 208 – remove "is evident."

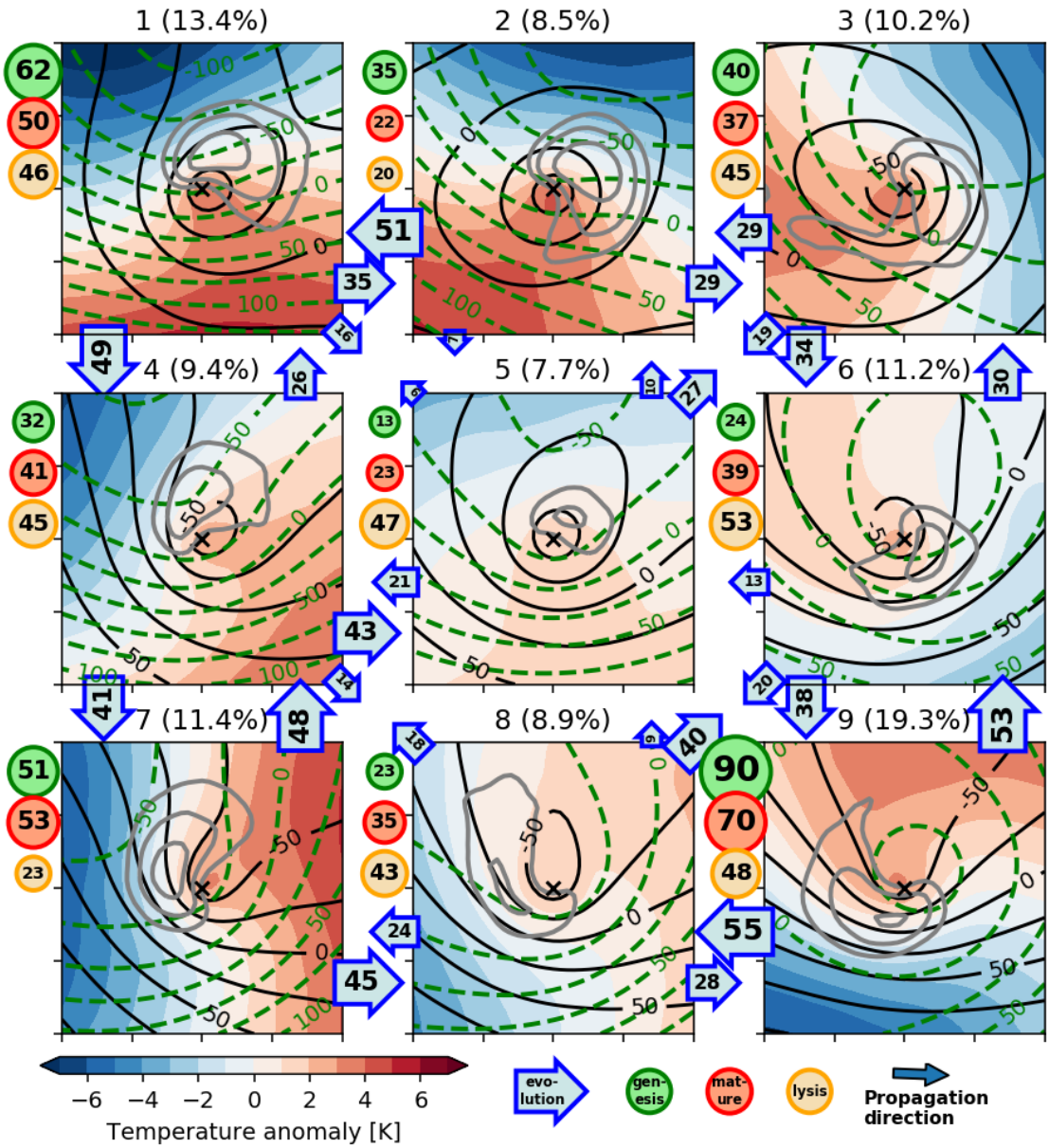

Figure 3: As Figure 2 of the manuscript, but without the back and forth removal of transitions.

Response: Done.

Reviewer: Line 218 – How was the medium-level cloud cover considered?

Response: See grey lines in Figure 2 of the manuscript. We slightly change the formulation: "Contours in high values in the medium-level cloud cover associated with each node have distinct patterns (Fig. 2)"
Reviewer: Line 256 – I would not call the pattern depicted in fig. 4 "a spectrum." Try to recall it.

Response: We changed the formulation: "Sorting all PLs by their shear in propagation and cross-propagation direction, a continuous 2-dimensional parameter space emerges.

Reviewer: Line 266 – "most likely intensify through the baroclinic instability."

Response: We do not understand the purpose of this comment.

Reviewer: Line 281 – I would rephrase this sentence as follows: "The strong shear is more common for time steps in the first half of the PL lifetime" since your version is a bit confusing:it seems like time steps are more common, while strong shear is more common.

Response: Thanks. We changed accordingly: "Strong shear is more common for time steps in the first half of the PL lifetime (Fig. 5c) and more often associated with a positive vorticity tendency, depicting intensification (Fig. 5d)."

Reviewer: Lines 282-283 – the same as for the previous comment: PL time steps are not "occurring" in the philosophical sense – it may be characterized by one or another shear condition.

Response: Indeed, we also adapted this: "In contrast, weak shear is most common at later stages and associated with decay (70%)."

Reviewer: Lines 281-287 – please rephrase the whole paragraph. Especially at lines 284-285, where you say that time steps are intensifying. I am sure that you meant that the PLs are intensifying at these time steps.

Response: We followed the recommendation and rephrased the paragraph: "Strong shear is more common in the first half of the PL lifetime (Fig. 5c) and more often associated with a positive vorticity tendency, depicting intensification (Fig. 5d). In contrast, weak shear is most common at later stages and associated with decay (70%). Even though some PL time steps in weak shear feature vortex intensification (30%), only for 6% of the weak-shear time steps the vortex is rapidly intensifying in the local-mean relative vorticity at a rate of more than $1 \times 10^{-5}\,\mathrm{s}^{-1}\,\mathrm{h}^{-1}$, whereas in strong-shear situations 22% of the time steps are associated to a vortex intensi-

fication exceeding this rate."

Reviewer: Lines 288-289 – Did you investigate the static stability parameter separately for that 30% of PLs within the weak-shear category, which are observed at the intensification stage? This may affect your main conclusion that the "convective" PLs are not presented in the STARS dataset.

Response: We did an investigation now and the static stability within the weak-shear category is similar for the intensifying and the decaying time steps (median value of 0.004462 and 0.004465 s^{-1}, respectively). As we state in the paragraph before, the 30% intensifying PLs in the weak-shear category are mainly close to the threshold to one of the strong shear categories and appear to be intensifying by baroclinic instability as well.

Reviewer: Line 312 – This statement is not fair enough. One would not expect the WISHE mechanism to be responsible for the intensification of PLs at the decaying stage (70% of time steps in this category); Secondly, it is known that the WISHE mechanism is effective at the mature stage of baroclinic MCs. For the "convective" PLs to create conditions for WISHE effect activation, it needs that the strong cyclonic circulation occurs.

Response: Could the reviewer provide some literature that demonstrate the effect of the WISHE mechanism in the mature stage of baroclinic MCs?

We did a new investigation and the surface heat fluxes within the weak-shear category is similar for the intensifying and the decaying time steps (median value of 202 and 198 W/m^2, respectively).
We clarified our formulation: "In the weak-shear category, surface fluxes are not exceptionally high, rendering it unlikely that the WISHE mechanism is more relevant for this category than for the strong-shear categories. However, also for the strong-shear categories surface fluxes appear to have a limited direct effects on the PL intensification (Sec. 4.2), questioning the relevance of the WISHE mechanism as being of primary importance for PL development."

Reviewer: Line 317 – Note that CAPE is the trigger mechanism that plays a larger role in the first half of the PL lifecycle, while the CISK is the process that occurs more in the second half (Emanuel and Rotunno, 1989), and it is better not to mix them up.

Response: We do not understand where we mix something up. The CISK mechanism is relying on CAPE as a reservoir of potential energy, which is also formulated in the article by Emanuel and Rotunno [1989]: "The authors have recently argued against CISK as a mechanism for tropical cyclogenesis (Emanuel, 1986; Rotunno and Emanuel, 1987). In the first place, when viewed in the proper thermodynamic framework, the tropical atmosphere is very nearly neutral to deep moist convection (Betts, 1982), presumably being maintained in the convectively adjusted state by

convection itself. The reservoir of available potential energy assumed by Charney and Eliassen (1964) and Ooyama (1964) in their original concept of CISK apparently does not exist in the tropical atmosphere."

Reviewer: Figure 6 caption – remove "within."

Response: Thanks.

Reviewer: Lines 336-344 – Saying "cold-air outbreak around Svalbard" (line 338) for forward-shear synoptic-scale condition and further "cold-air outbreak to the west of Svalbard" (line 341) for reverse-shear PLs, you confuse the reader because these descriptions are partly overlapping. Looking at fig.7, one may notice that the direction of the cold-air outbreak and isotherms inclination is very different for two of these cases. Thus, I would pay more attention to the text on these differences than say that both types of shear forms, particularly under the same conditions. For example, reverse-shear conditions are linked to the cold-air outbreaks over the Norwegian Sea, having the north-east direction of the mean flow, while forward-shear conditions are more about the CAO in the Barents Sea, with the mean flow directed west-north-westward.

Response: Thanks, we changed the formulation of the first two paragraphs of this section: "Within the Nordic Seas, each of the shear categories is associated with a distinct synoptic-scale situation (Fig. 7), leading to typical locations and propagation directions of PLs within each shear category. Forward-shear conditions often form south or south-west of a synoptic-scale low-pressure system, located in the northern Barents Sea (Fig. 7a). The synoptic low causes a marine cold-air outbreak on its western side and a zonal flow further downstream on its southern side almost along the isotherms. Forward-shear PLs most frequently occur in this zonal flow and consequently propagate eastward.
The synoptic-scale situation for reverse-shear PLs mainly features a low-pressure system over northern Scandinavia leading to a cold-air outbreak from the Arctic to the Norwegian Sea, where most reverse-shear PLs develop (Fig. 7c). The flow in which reverse-shear PLs typically occur is south-westward, consistent with their direction of propagation almost along the isotherms, though with the cold side on the opposite side as seen from the direction of propagation of forward-shear PLs. The most frequent location and propagation direction of forward and reverse-shear PLs is in accordance with Terpstra et al. [2016] and Michel et al. [2018]."

Reviewer: Line 345 – "occur south of Svalbard" instead of "occur to the south of Svalbard."

Response: Thanks.

Reviewer: Line 344 In addition to lines 336-344 – Here, left-shear conditions are typical in cold-air outbreaks with northward mean flow. This is its main difference from what we see in fig.7 for forward-shear.

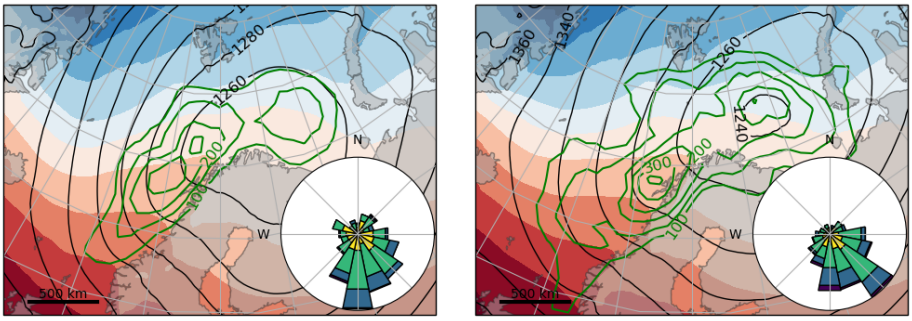

(a) weak shear intensifying (b) weak shear decaying

Figure 4: As Figure 7 of the manuscript. (a) only intensifying, and (b) only decaying PLs in the weak-shear category.

Response: We reformulate this paragraph: "In left-shear conditions, a low pressure system is located over the Barents Sea causing a south to south-eastward directed cold-air outbreak across the isotherms towards a warmer environment (Fig. 7d). Hence, left-shear PLs primarily occur south of Svalbard at the leading edge of the cold-air outbreak."

Reviewer: Lines 348-352 – The weak-shear category is still looking not enough investigated. Fig.7e shows very clearly two types of patterns of PLs occurrence under this category. One of those is naturally the lysis near the east coast of Greenland. However, the second, which is less numerous, should represent that 30% of generated PLs correspond to the upper-level PV anomaly-induced development of the PLs (see RT2003, chapter 4.4, or Bracegirdle and Gray, 2007).

Response: Figure 7 display the track density of PLs in weak shear category associated to intensifying (a) and decaying (b) situations. The distribution of their locations is similar and it does not appear as if one pattern of Figure 7e of the manuscript belongs to intensifying and the other to decaying time steps.
We interpret that the "upper-level PV anomaly-induced development of the PLs" is also following a baroclinic arrangement.

Reviewer: Line 380 – need to add a citation for the CISK mechanism realization, such as Charney and Eliassen, 1964; Rasmussen 1979; Businger and Reed, 1984; or any other that you prefer.

Response: We interpret that the contribution of latent heating is best explained within a moist baroclinic framework, instead of the CISK mechanism. We formulate this more clearly and add a citation: "The release of latent heat associated with the precipitation leads to the production of potential vorticity underneath the level of strongest heating and hence intensifies the low-level circulation within a moist-baroclinic framework [Balasubramanian and Yau, 1996; Kuo et al., 1991]."
We could not find an article by Businger and Reed from the year 1984.

Reviewer: Figure 9 – (b) instead of (b, c)

Response: Thanks.

Reviewer: Line 399 – check the citation.

Response: We did.

Reviewer: Line 405 – "which is actually" instead of "is actually."

Response: We set a comma instead.

References

G Balasubramanian and MK Yau. The life cycle of a simulated marine cyclone: Energetics and pv diagnostics. *Journal of the atmospheric sciences*, 53(4):639–653, 1996.

Christopher A Davis and Kerry A Emanuel. Potential vorticity diagnostics of cyclogenesis. *Monthly weather review*, 119(8):1929–1953, 1991.

Kerry A Emanuel and Richard Rotunno. Polar lows as arctic hurricanes. *Tellus A*, 41(1):1–17, 1989.

Gunther Heinemann and Chantal Claud. Report of a workshop on" theoretical and observational studies of polar lows" of the european geophysical society lows working group. *Bulletin of the American Meteorological Society*, 78(11):2643, 1997.

Ying-Hwa Kuo, MA Shapiro, and Evelyn G Donall. The interaction between baroclinic and diabatic processes in a numerical simulation of a rapidly intensifying extratropical marine cyclone. *Monthly Weather Review*, 119(2):368–384, 1991.

Clio Michel, Annick Terpstra, and Thomas Spengler. Polar mesoscale cyclone climatology for the nordic seas based on era-interim. *Journal of Climate*, 31(6): 2511–2532, 2018.

Erik A Rasmussen and J Turner. *Polar lows: Mesoscale Weather Systems in the Polar Regions*. Cambridge University Press, 2003.

Maxence Rojo, Chantal Claud, Paul-Etienne Mallet, Gunnar Noer, Andrew M Carleton, and Marie Vicomte. Polar low tracks over the nordic seas: a 14-winter climatic analysis. *Tellus A*, 67, 2015.

Julia E Smirnova and Pavel A Golubkin. Comparing polar lows in atmospheric reanalyses: Arctic system reanalysis versus era-interim. *Monthly Weather Review*, 145(6):2375–2383, 2017.

Mark T Stoelinga. A potential vorticity-based study of the role of diabatic heating and friction in a numerically simulated baroclinic cyclone. *Monthly weather review*, 124(5):849–874, 1996.

Patrick J Stoll, Rune G Graversen, Gunnar Noer, and Kevin Hodges. An objective global climatology of polar lows based on reanalysis data. *Quarterly Journal of the Royal Meteorological Society*, 144(716):2099–2117, 2018.

Patrick J. Stoll, Teresa M. Valkonen, Rune G. Graversen, and Gunnar Noer. A well-observed polar low analysed with a regional and a global weather-prediction model. *Quarterly Journal of the Royal Meteorological Society*, 146(729):1740–1767, 2020.

Annick Terpstra, Clio Michel, and Thomas Spengler. Forward and reverse shear environments during polar low genesis over the north east atlantic. *Monthly Weather Review*, 144(4):1341–1354, 2016.

Wataru Yanase, Gang Fu, Hiroshi Niino, and Teruyuki Kato. A polar low over the japan sea on 21 january 1997. part ii: A numerical study. *Monthly Weather Review*, 132(7):1552–1574, 2004.

Polar Lows – Moist Baroclinic Cyclones Developing in Four Different Vertical Wind Shear Environments

Patrick Johannes Stoll[1], Thomas Spengler[2], Annick Terpstra[2], and Rune Grand Graversen[1,3]

[1]Department of Physics and Technology, Arctic University of Norway, Tromsø, Norway
[2]Geophysical Institute, University of Bergen, and Bjerknes Centre for Climate Research, Bergen, Norway
[3]Norwegian Meteorological Institute, Norway

Correspondence: Patrick Johannes Stoll (patrick.stoll@uit.no)

Abstract. Polar lows are intense mesoscale cyclones that develop in polar marine air masses. Motivated by the large variety ~~in~~ of their proposed intensification mechanisms, cloud structure, and ambient sub-synoptic environment, we use self-organising maps to classify polar lows. The method is applied to 370 polar lows in the North-East Atlantic, which were obtained by matching mesoscale cyclones from the ERA-5 reanalysis to polar lows registered in the STARS dataset by the Norwegian Meteorological Institute~~in the STARS dataset~~. ERA-5 reproduces ~~93%~~ most of the STARS polar lows.

We identify five different polar-low configurations ~~,~~ which are characterised by the vertical wind shear vector, the change of the horizontal-wind vector with height, relative to the propagation direction. Four categories feature a strong shear with different orientations of the shear vector, whereas the fifth category contains conditions with weak shear. ~~The orientation of the vertical-shear vector for the strong shear categories determines the dynamics of the systems, confirming~~ This confirms the relevance of ~~the~~ a previously identified categorisation into forward and reverse-shear polar lows. ~~In addition, we~~ We expand the categorisation with right and left-shear polar lows that propagate towards colder and warmer environments, respectively.

~~Polar lows in the four strong shear categoriesfeature an up-shear tilt in the vertical, typical for~~ For the strong-shear categories, the shear vector organises the moist-baroclinic dynamics of the systems. This is apparent in the low-pressure anomaly tilting with height against the shear vector, and the main updrafts occurring along the warm front located in the forward-left direction relative to the shear vector. These main updrafts contribute to the intensification through ~~moist baroclinic processes. As weak-shear conditions mainly occur at the mature or lysis stage of polar lows, we~~ latent-heat release and are typically associated with comma-shaped clouds.

Polar low situations with a weak shear, that often feature spirali-form clouds, occur mainly at decaying stages of the development. We thus find no evidence for hurricane-like ~~development and propose~~ intensification of polar lows and propose instead that spirali-form ~~PLs are most likely~~ clouds are associated with a warm seclusion process.

1 Introduction

Polar lows (PLs) are intense mesoscale cyclones with a typical diameter of 200 - 500 km and a short lifetime of 6 - 36 h that develop in marine cold-air outbreaks during the extended winter season (e.g Rasmussen and Turner, 2003; Yanase et al., 2004; Claud et al., 2004; Renfrew, 2015; Rojo et al., 2015). Despite ~~numerical-weather prediction (NWP)~~ numerical

weather-prediction models being capable ~~to simulate~~ of simulating these systems, operational forecasts still have have issues predicting the exact location and intensity of PLs (e.g. Kristjánsson et al., 2011; Føre et al., 2012; Stoll et al., 2020). Several paradigms have been proposed to describe PL development, ranging from baroclinic instability (e.g. Harrold and Browning, 1969; Reed, 1979; Reed and Duncan, 1987) to symmetric hurricane-like growth (e.g. Rasmussen, 1979; Emanuel and Rotunno, 1989). The multitude of paradigms demonstrates that our dynamical interpretation of these systems is still ~~lacking~~ deficient (Jonassen et al., 2020). To further alleviate this shortcoming, we present a classification of PLs by their structure and sub-synoptic environment to identify the relevance of the proposed paradigms.

The proposed PL paradigms often stem from the different cloud structures (Forbes and Lottes, 1985; Rojo et al., 2015) and sub-synoptic environments (Duncan, 1978; Terpstra et al., 2016). From the 1980s, the PL spectrum was thought to range from pure baroclinic PLs with a comma-shaped cloud structure to convective systems with a spirali-form cloud signature like hurricanes (p.157 Rasmussen and Turner, 2003). The latter ~~usually~~ types usually were argued to be invoked either conditional instability of the second kind (CISK Charney and Eliassen, 1964; Ooyama, 1964) or ~~wind induced~~ by wind-induced surface heat exchange (WISHE Emanuel, 1986)~~as mechanisms for intensification~~. However, most PLs appear as hybrids between the ~~ends~~ extremes of this spectrum (Bracegirdle and Gray, 2008).

Using idealised simulations to map the sensitivities of cyclone development in ~~this~~ the PL spectrum, Yanase and Niino (2007) found that cyclones intensify fastest in an environment with high baroclincity ~~,~~where latent heat release supports the development. ~~Thus, PLs are mostly characterised by moist baroclinic instability and~~ As neither dry baroclinic nor pure CISK modes grow fast enough to explain ~~their development~~ the rapid intensification of PLs, the growth is most likely associated with moist baroclinic instability (Sardie and Warner, 1983; Terpstra et al., 2015).

Furthermore, hurricane-like PLs ~~do usually not~~ rarely resemble the structure of hurricanes~~and instead~~ ; instead they feature asymmetric updrafts typical of baroclinic development with latent heating not playing the dominant role (Føre et al., 2012; Kolstad et al., 2016; Kolstad and Bracegirdle, 2017). The PLs that appear hurricane-like in their mature stage ~~were also observed~~ appear to be initiated by baroclinic instability (e.g. Nordeng and Rasmussen, 1992; Føre et al., 2012).

Several categorisations of PLs were proposed to shed light on the development pathways of PLs (e.g. Duncan, 1978; Businger and Reed, 1989; Rasmussen and Turner, 2003; Bracegirdle and Gray, 2008; Terpstra et al., 2016). Duncan (1978) suggested a categorisation based on the vertical ~~wind shear~~ wind-shear angle of the PL environment, defined as the angle between the tropospheric mean wind vector and the thermal wind vector. Situations where the vectors point in the same (opposite) direction are referred to as forward (reverse) shear conditions. PLs have been found to occur in both forward-shear (e.g. Reed and Blier, 1986; Hewson et al., 2000) and reverse-shear environments (e.g. Reed, 1979; Bond and Shapiro, 1991; Nordeng and Rasmussen, 1992), where both types of PLs occur approximately equally often (Terpstra et al., 2016).

PLs in forward-shear environments develop similar to typical mid-latitude cyclones in a deep-baroclinic zone with an associated upper-level jet. They have the cold air to the left with respect to their direction of propagation and are mainly propagating eastward (Terpstra et al., 2016). PLs in reverse-shear environments, on the other hand, often develop in the vicinity of an occluded ~~low pressure~~ low-pressure system and are characterised by a low-level jet. They have the cold air to the right with respect to their propagation direction and are mainly propagating southward. Reverse-shear PLs also feature considerably

higher surface heat fluxes and a lower static stability in the troposphere, expressed by a larger temperature contrast between the temperature at the sea surface and at 500 hPa (Terpstra et al., 2016).

However, assigning PL environments solely based on two types of shear conditions might be insufficient to characterise ~~PLs. Furthermore, the~~ all PLs types. The shear angle cannot distinguish between baroclinically- and convectively-driven systems, hence it cannot address the hurricane-like part of the PL spectrum. To alleviate this shortcoming, we categorise PLs based on their sub-synoptic environment using self-organising maps (SOM, see Section 2.5)~~without an *a-priori* determination of a variable used for the categorisation~~. The thereby identified meteorological configurations reveal the underlying PL intensification mechanisms, allowing us to investigate the following research questions:

- What are the archetypal meteorological conditions during PL development?
- Can the existing PL classification be confirmed or should it be revised?
- What are the pertinent intensification mechanisms?

2 Methods

2.1 Polar-low list

This study is based on the Rojo list (Rojo et al., 2019), a modified version of the STARS (Sea Surface Temperature and Altimeter Synergy for Improved Forecasting of Polar Lows) dataset~~(Rojo et al., 2019, henceforth Rojo list)~~. This list includes the location and time of PLs detected from AVHRR satellite images over the North-East Atlantic that were listed in the STARS dataset by the Norwegian Meteorological Institute between November 1999 and March 2019 (Noer and Lien, 2010). The STARS dataset has been used for several previous PL studies (e.g. Laffineur et al., 2014; Zappa et al., 2014; Rojo et al., 2015; Terpstra et al., 2016; Smirnova and Golubkin, 2017; Stoll et al., 2018).

The advantage of the Rojo list compared to the STARS dataset is that it contains considerably more ~~PLs~~PL cases. While the STARS dataset only ~~contains~~ includes the major PL ~~in situations~~ centre for events of multiple PL developments, the Rojo list includes the location of all individual ~~PLs~~ PL centres (Rojo et al., 2015). Thus, the Rojo list includes 420 ~~PLs~~PL centres, which are associated with the 262 PL events in the STARS database of which 183 PL events feature a single PL centre and the remaining 79 events have 2 - 4 ~~PLs~~ PL centres per event. In addition, the Rojo list classifies the cloud morphology for each detected PL time step.

As the Rojo list includes individual time steps of each PL when AVHRR satellite images were available, the time interval between observations is irregular and ranges ~~between~~ from 30 minutes and up to 12 hours. This also implies that the list in many cases lacks the genesis and lysis time of some PLs.

2.2 Polar-low tracks in ERA-5

We use ~~fields from~~ the European Centre for Medium-Range Weather Forecasts (ECMWF) state-of-the-art reanalysis version 5 (ERA-5 Hersbach and Dee, 2016) to track PLs and analyse the atmospheric environment. The ability of ERA-5 to simulate PLs has not yet been investigated, though some studies have shown that atmospheric models with a comparable horizontal resolution to ERA-5 are capable to produce most PL cases (Smirnova and Golubkin, 2017; Stoll et al., 2018). Further, Stoll et al. (2020) demonstrated that the ECMWF model at comparable resolution as ERA-5 reproduced the 4 dimensional structure of a particular PL case reasonably well. As other studies estimated the amount of represented STARS PLs in ERA-Interim~~to~~ , the precursor reanalysis to ERA-5, to be 48% Smirnova and Golubkin (2017), 55% (Zappa et al., 2014), 60% (Michel et al., 2018), and 69% (Stoll et al., 2018), we anticipate the performance of ERA5 to be even higher. Note that this study does not rely on a realistic reproduction of the PLs, as we mainly focus on the PL environment that has a spatial scale that is well captured by ERA-5.

The ERA-5 model provides data from 1950 to the near-present at hourly resolution with a spectral truncation of T639 in the horizontal direction, which is equivalent to a grid spacing of about 30 km. The ~~data~~ reanalysis has 137 hybrid levels in the vertical, of which approximately 47 are below 400 hPa, which is the typical height of the tropopause ~~at high latitudes~~in polar-low environments (Stoll et al., 2018). We obtained the data at a lat $\times$ lon grid of $0.25° \times 0.5°$ within 50° - 85°N and 40°W - 65°E. We chose a coarser grid spacing for the longitudes due to their convergence towards the pole. ~~We use data from the surface and from the pressure levels at 925, 850, 700 and 500 .~~

To analyse the PL development, we derive PL tracks with an hourly resolution by applying the mesoscale tracking algorithm developed by Watanabe et al. (2016) and retain the tracks that match the Rojo list. The tracking procedure is based on detecting local maxima in relative vorticity at 850 hPa, where we tuned the parameters in the tracking algorithm ~~with~~ based on the objective to obtain a good match with the Rojo list.

In particular, we modified the algorithm as follows:

- No land mask is applied ~~to account for~~ in order to include PLs propagating partially over land.
- A uniform filter with a 60 km radius is applied to the relative vorticity to reduce artificial splitting of PL tracks and to smooth the tracks.
- ~~The threshold for~~ Parameters in the algorithm by Watanabe et al. (2016) are adapted; the vortex peak to $\zeta_{max,0}$ is $1.5 \cdot ~~10^{-4}~~ \times 10^{-4}\,\mathrm{s}^{-1}$, and the ~~threshold for the vortex area~~ vortex area to $\zeta_{min,0}$ is $1.2 \cdot ~~10^{-4}~~ \times 10^{-4}\,\mathrm{s}^{-1}$.
- We do not require a filter for synoptic-scale disturbances, as the matching to the Rojo list ensures that the tracks include PLs only.

All tracks that have a distance of less than 150 km to a PL from the Rojo list for at least one time step are regarded as matches. ~~Hereby, 374 of the 420 PL centres from the Rojo list have at least one associated PL track. In total , however,~~ In total we obtain 556 associated PL tracks~~, where multiple~~ . Multiple matches to the same PL from the Rojo list ~~have two reasons.~~ occur due to two reasons: Firstly, ERA-5 features multiple PLs connected to ~~the~~ one PL centre from the Rojo list. Secondly,

the tracking algorithm yields several track segments for the same PL. The latter occurs if the location of the vorticity maximum moves within an area of high vorticity, e.g., a frontal zone. In these cases, two track segments are merged ~~if~~ provided that the time gap between them is less than 6 hours~~and if~~ , and that the extrapolation of one track segment over the time gap includes the other segment within a distance of 150 km. This merging was applied for 86 PL tracks, such that 470 PL tracks remain.

We exclude tracks ~~if the lifetime is~~ having a lifetime shorter than 5 hours (54 tracks) and ~~if the track is~~ being located over land for most of the PL lifetime (5 tracks). The latter is defined as when the initial, middle, and final time step of the PL ~~occurring~~ all occur on land. Other land exclusion methods were tested and gave similar results. If a track is included twice, which occurs when it matches with two PLs from the Rojo list, one is removed (37 tracks), and is labelled as a match to both PLs from the Rojo list.

Applying this procedure, a total of 374 ~~of the total~~ out of the initial 556 PL tracks is retained with 13,221 hourly time steps. ~~These 374 PLs~~The list with the obtained PL tracks is provided in the supplement. We compared a random subset of obtained tracks with the PLs from the Rojo list, satellite imagery, and ERA-5 fields and concluded that the vast majority of the obtained tracks can be considered to be PLs. The results of this study were further found to be qualitatively insensitive to the exact settings in the track matching and exclusion procedures.

The number of detected PL tracks (374) is close to the number of PL centres included in the Rojo list (420). The 374 PL tracks are associated with ~~243~~ 244 different PL events from the Rojo list~~. Hence, 243~~ , implying that 244 of the 262 PL events (93%) from the Rojo list are ~~matched to cyclones~~ reproduced in ERA-5~~and the number of detected PL tracks~~ . These 374 PL tracks are associated with 348 different PL centres from the Rojo list. As mentioned earlier, sometimes multiple PLs are observed in ERA-5 associated to one PL from the Rojo list, which appears realistic after investigating these cases, as also the Rojo list misses some PL centres.

In total, for 348 of the 420 centres (83%) from the Rojo list at least one associated PL is found. In the Norwegian Sea, 219 of 255 (~~374) is close to the number of PLs included~~ 86%) PL centres from the Rojo list ~~(420) . This highlights~~ are reproduced, whereas 129 of 165 (78%) are detected in the Barents Sea, where PLs in the Norwegian and Barents Sea are separated by the longitude of the first time step being smaller or larger than 20° E, respectively. A higher detection rate of STARS PLs for the Norwegian than for the Barents Seas was also observed by Smirnova and Golubkin (2017). It may be explained by STARS PLs being larger in the former than in the latter ocean basin (Rojo et al., 2015) and larger systems being more likely captured by ERA-5. The high detection rates indicate the capability of ERA-5 to represent most ~~PL events and that the applied tracking and matching procedure is successful. Furthermore, our detection rate indicates~~ PLs and highlights that ERA-5 is superior to its predecessor ERA-Interim when it comes to capturing PLs, where Stoll et al. (2018) detected 55% and Michel et al. (2018) about 60% of the STARS PLs in ERA-Interim. Note that the ~~match rates strongly depends~~ detection rates depend on the applied matching criteria. The matching criteria applied here ~~is stronger than the one~~ are stronger than those applied in Stoll et al. (2018).

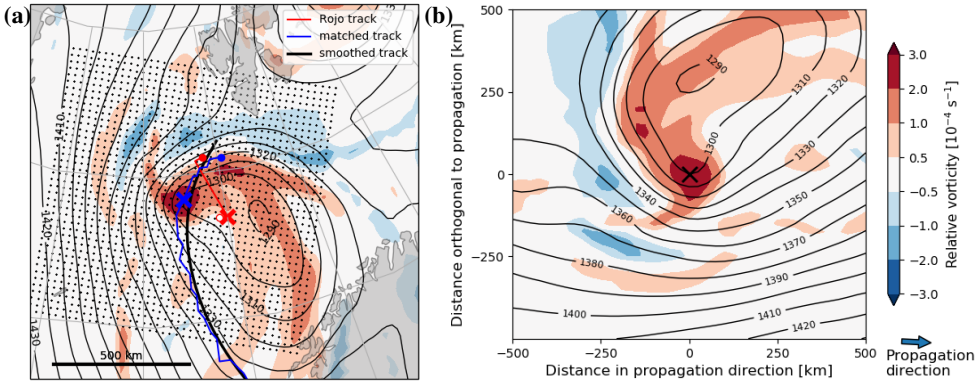

Figure 1. Exemplary depiction of deriving the PL-centred analysis. (a) Relative vorticity at 850 hPa (shading) and geopotential height at 850 hPa (contours, spacing 10 m) for 20 March 2001 01:00 UTC. The track of polar low number 10 from the Rojo list is shown in red and the matched track is depicted in blue. The location at the selected time are indicated by ~~squares~~'x'. The smoothed track is depicted in black, the propagation direction of the PL at the selected time is southward. ~~The location of the grid cells of the polar-low centred analysis domain are denoted by black dots.~~ (b) Same fields as for (a) in the polar-low centred domain, constructed such that the polar-low centre is in the middle (~~black~~ 'x') and the propagation direction is towards the right.

2.3 Polar-low centred analysis

We employ a PL-centred analysis, where meteorological fields from ERA-5 for each individual time step of a PL track are transformed onto a PL-centred grid. The cells of the PL-centred grid (black dots in Figure 1) are derived from the location and propagation direction of the PL. The propagation direction is obtained by applying a cubic-spline smoothing to the PL track points (De Boor, 1978). We smooth, because the tracks can feature non-monotonous behaviour due to the discrete nature of the grid and varying locations of the vorticity maxima in areas of enhanced vorticity, such as frontal zones. Smoothing also provides continuous tracks in situations of low propagation speed, where the propagation direction is highly variable.

~~All meteorological~~ Meteorological fields from ERA-5 were linearly interpolated onto the PL-centred grid with an extent of 1000×1000 km, and with a grid spacing of 25 km (see Fig. 1). Given a typical PL diameter between 150 and 600 km (Rojo et al., 2015), this grid covers the PL and its sub-synoptic environment.

We exclude time steps where this grid is not fully within the chosen ERA-5 boundaries (Section 2.2). This reduces the PL time steps from 13,221 to 12,695 and removes 4 of the 374 PLs for their complete lifetime. As most of the excluded time steps occur at the end of the PL lifetime, this exclusion has ~~only a small~~ insignificant influence on our analysis of the PL intensification.

2.4 Parameter preparation

In addition to standard meteorological variables, we derived an additional set of parameters using grid points within a radius of 250 km around the PL centre. For near-surface parameters, such as the 10 m wind vector, the turbulent heat fluxes, and

parameters partly derived from low-levels, such as the Brunt-Väisälä frequency, only grid cells over open ocean, defined by a water fraction larger than 80%, are included. Presented results were found qualitatively insensitive to variations in the radius.

We estimate the tropospheric **Brunt-Väisälä frequency**, N, using the potential temperature, θ, at 500 and 925 hPa

$$N = \sqrt{\frac{g}{\overline{\theta}}\frac{\partial\theta}{\partial z}} \approx \sqrt{\frac{g}{(\theta_{500}+\theta_{925})/2}\frac{\theta_{500}-\theta_{925}}{z_{500}-z_{925}}} \tag{1}$$

with gravitational constant $g = 9.8\,\mathrm{ms}^{-2}$ and geopotential height z. Afterwards, we apply a radial average to obtain the environmental value.

The **differential wind vector** is computed using the mean wind vectors at 500 and 925 hPa,

$$\Delta\overline{\boldsymbol{u}} = (\Delta\overline{u}, \Delta\overline{v}) = (\overline{u_{500}} - \overline{u_{925}}, \overline{v_{500}} - \overline{v_{925}}), \tag{2}$$

where an overbar indicates the mean computed within a radius of 500 km around the PL centre. The upper-level (500 hPa) is considerably higher than the level ~~chosen by Terpstra et al. (2016)~~ (700 hPa) chosen by Terpstra et al. (2016). Given that PLs span the entire depth of the polar troposphere, we chose one level from the lower and one from the upper troposphere, with neither level intersecting with the sea surface ~~or~~ nor the tropopause.

We define the **vertical-shear strength** as

$$\left|\frac{\Delta\overline{\boldsymbol{u}}}{\Delta\overline{z}}\right| = \frac{|\Delta\overline{\boldsymbol{u}}|}{\overline{z_{500}} - \overline{z_{925}}}. \tag{3}$$

The **vertical-shear angle**, $\alpha = [\alpha_s - \alpha_p]\,(\mathrm{mod}\ 360°)$, is derived from the angle between the differential wind vector, $\Delta\overline{\boldsymbol{u}}$, and the propagation direction, α_p, of the PL. The propagation vector of the PL appears to be a good estimate of the mean wind encountered by the PL (Fig. 3). Different to Terpstra et al. (2016), we compute the radial average before calculating the angle. Thereby, our method obtains the shear angle of the environmental mean flow and partially filters for perturbations induced by the PL itself. Also to reduce the influence of the PL-induced perturbations, a large radius of 500 km is applied for the computation of the differential wind vector. Note, that the shear angle by this computation takes values between 0 and 360° and not between 0 and 180° as in Terpstra et al. (2016). In addition, we define the **vertical-shear vector** in the propagation direction

$$\left(\frac{\Delta\overline{\boldsymbol{u}}}{\Delta\overline{z}}\right)_p = \left|\frac{\Delta\overline{\boldsymbol{u}}}{\Delta\overline{z}}\right| \cdot (\cos(\alpha), \sin(\alpha))\,. \tag{4}$$

Our method is different to Duncan (1978) and Terpstra et al. (2016), though tests confirm that their thermal wind vector is qualitatively similar to the vertical-shear vector utilised in this study.

The **vorticity tendency** of ~~the PL time steps~~ a PL time step is obtained from the first derivative in time of the vorticity maxima that was used for the detection of the PL. These maxima are based on the spatially-smoothed vorticity using a uniform filter of 60 km radius (point two of the algorithm modifications in Sec. 2.2). However, the time evolution in the vorticity is still discontinuous (~~see Supplementary figure~~Supplementary Fig. 1). Therefore a Savitzky-Golay filter (Savitzky and Golay, 1964) is applied on the time evolution in the vorticity for the computation of the first derivative. This filter applies a least-square

regression in our case of a second-order polynomial within a window of eleven vorticity time steps, or ~~the whole lifetime if it~~ of the whole PL lifetime if this is shorter than ten hours. The **growth rate** is computed by the fraction of the vorticity tendency to the vorticity of ~~an~~ a time step.

2.5 Self-organising maps (SOM)

Kohonen (2001) developed the SOM method for displaying typical patterns in high-dimensional data. The patterns, also referred to as nodes, are ordered in a 2-D array with neighbouring nodes being more similar to each other than nodes ~~with a longer distance~~ further apart in the array. Kohonen (2001) originally developed the method for artificial neural networks, but in recent years it has been extensively applied in many fields of science~~in the last years~~, including climate data analysis (e.g. Nygård et al., 2019).

We apply the package described in Wehrens et al. (2007)~~for the computation~~. The size of the node array has to be subjectively ~~determined~~ chosen for the dataset at hand and is typically determined after some testing. We find an array of 3×3 nodes to be most suitable, reducing 12,695 PL-centred fields to 3×3 archetypal nodes. Larger arrays mainly display additional details of minor interest (Supplementary ~~Figure~~Fig. 2), whereas smaller arrays merge nodes that contained relevant individual information.

~~We chose~~ The SOM analysis is based on the temperature anomaly field at 850 hPa of each time step ~~$T'(x,y) = T(x,y) - \overline{T}(x,y)$ as a basis for the SOM analysis~~$T'(x,y) = T(x,y) - \overline{T}$, with $\overline{T}$ denoting the local mean temperature within the PL-centred grid of a given time step. In this way, the ~~information if a PL occurred~~ fields become independent on the PL occurring in a relatively warm or cold environment~~is removed~~, which would otherwise dominate the SOM analysis (Supplementary ~~Figure~~Fig. 3 and 4). Thereby, the intrinsic temperature structure ~~is most apparent. We also applied~~ becomes apparent. In order to illustrate the robustness of the result, we also apply the SOM algorithm to several other atmospheric fields~~, which are presented and discussed in the supplementary material section 3.~~. The SOM matrices produce similar patterns of variability when applied to the temperature anomaly field at other levels, the specific humidity anomaly, and the upper and lower-level geopotential height anomaly (~~see supplementary material~~Supplement Section 3). This demonstrates the generality of the results obtained from the temperature anomaly field at 850 hPa. Additionally, Supplement Section 5 provides evidence that the SOM algorithm is successful in detecting characteristic PL environments.

An advantage of the orientation of the PL-centred fields ~~by~~ based on the propagation direction is a reduction of the variability in the mid-level flow, as ~~the mid-level~~ this flow largely determines the propagation of the PLs. Therefore, the SOM matrix obtained using the mid-level geopotential height anomaly produce nodes that are ~~quite~~ fairly similar to each other (~~see Supplementary Figure~~Supplementary Fig. 7)~~. This expresses a small variability among PLs based on this variable and~~ , which expresses that PLs are generally characterised by a mid-level trough within a background flow in the propagation direction of the PL.

The ~~time steps within each node can be associated with different PL phases, such as genesis , maturity~~PL time steps associated with genesis (intial), mature, and lysis ~~.~~ (last) stages are counted for each node. The mature stage of the PL is here defined as the time step with the maximum spatially-filtered relative vorticity at 850 hPa, as utilised in the tracking algo-

rithm (~~see Supplementary Figure~~ Supplementary Fig. 1). A PL can transition through several SOM nodes during its lifetime, which can be tracked through the SOM matrix. Evolution primarily occurs between neighbouring SOM nodes, as neighbours in the SOM matrix are most similar. Sometimes PLs transition back and forth between nodes, which ~~means~~ indicates that the system is in a state between two nodes. We ~~remove~~ disregard this back and forth development as it does not express a clear transition of the system.

3 Typical polar-low configurations

3.1 Patterns of variability

The SOM nodes have horizontal temperature anomaly fields resembling different strength and orientation of the temperature gradient with respect to the propagation direction of the PLs (Fig. 2). Nodes in the corners are the most extreme by construction of the SOM algorithm and therefore include the strongest horizontal temperature gradients. Nodes on opposing sides of the matrix display temperature anomaly fields that are most different from each other.

PLs in SOM node 1 and 9 propagate approximately perpendicular to the horizontal temperature gradient at 850 hPa with the cold side to the left and right, respectively, of the propagation direction. Thus, nodes 1 and 9 represent the classical forward and reverse-shear conditions, respectively (e.g. Forbes and Lottes, 1985; Terpstra et al., 2016). The other two nodes in the corner of the SOM matrix, node 3 and 7, also feature a large horizontal temperature gradient. PLs in node 3 are propagating towards lower temperatures. The opposite ~~is evident~~ in node 7 with PLs propagating towards higher temperatures. The remaining nodes display intermediate ~~states~~ situations with weaker temperature gradients~~, where~~. Note that none of the nodes resemble axis-symmetric characteristics that would be typical for hurricane-like PLs.

The nodes have characteristic upper (500 hPa) and lower-level (1000 hPa) flow fields (Fig. 2), where PLs in node 1 have a closed low-level circulation and an upper-level trough located ~~up-shear~~upstream (to the left of the PL centre in the depiction of Fig. 2). PLs in node 9 feature a low-level trough and a closed upper-level circulation slightly downstream. PLs in node 3 feature a weaker low-level circulation and a weak upper-level trough positioned slightly ~~up-shear~~to the left of the direction of propagation. Node 7 ~~feature~~ features a short-wave low-level trough with an axis tilted from the PL centre to the left and downstream of the propagation direction, whereas the upper levels feature a trough ~~located up-shear~~ with an axis to the left and upstream of the direction of propagation. ~~PLs in node 9 have a closed and weak upper-level circulation and a low-level trough slightly up-shear of the upper-level circulation with an axis oriented to the left of the direction of propagation.~~

~~The~~ Contours in high values in the medium-level cloud cover associated with each node has ~~a distinct distribution and location of its maximum~~ distinct patterns (Fig. 2), which coincides with the region where the main updrafts occur (not shown). ~~All nodes have a comma-shaped~~ The medium-level cloud cover ~~with a different orientation, typically~~ forms a comma shape with different orientation for each node. The cloud is typically located along the warm front on the cold side of the PL centre.

PLs transition between SOM nodes during their life cycle (Fig. 2), which means that the orientation of the environmental flow as compared to the thermal field can change for an individual PL. Also the strength of the environmental temperature gradient varies. At genesis times (green circles in Fig. 2), PLs are most frequently associated with the SOM nodes in the corners (Fig. 2).

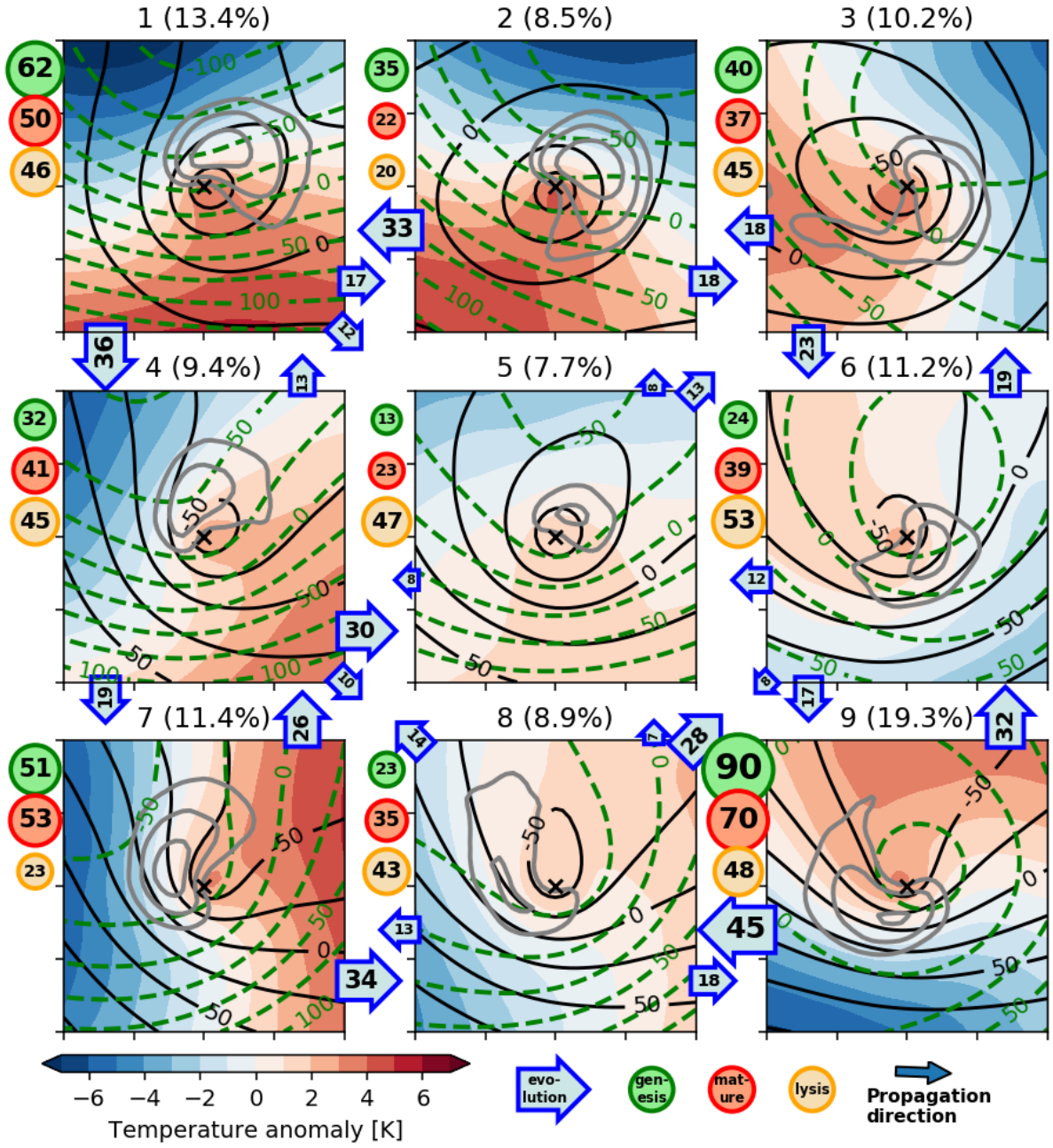

Figure 2. The self-organising map based on the 850 hPa temperature anomaly (T') using 12,695 PL time steps in a PL-centred grid as derived in Figure 1. The black 'x' marks the PL centre, ticks on x and y-axis are spaced at 250 km. Displayed is the composite of the 850 hPa temperature anomaly (shading), 1000 hPa geopotential height anomaly (black contours, spacing 25 m), 500 hPa geopotential height anomaly (green dashed contours, spacing 25 m) and medium-level cloud-cover fraction (grey contours at 0.7, 0.8 and 0.9). The number labels the SOM nodes and the percentage of time steps represented by the respective node. Green, red, and yellow circles indicate the number of genesis, mature, and lysis stages within each node. The numbers in the arrows indicate the amount of transitions between two nodes, where numbers smaller than 5 are not displayed.

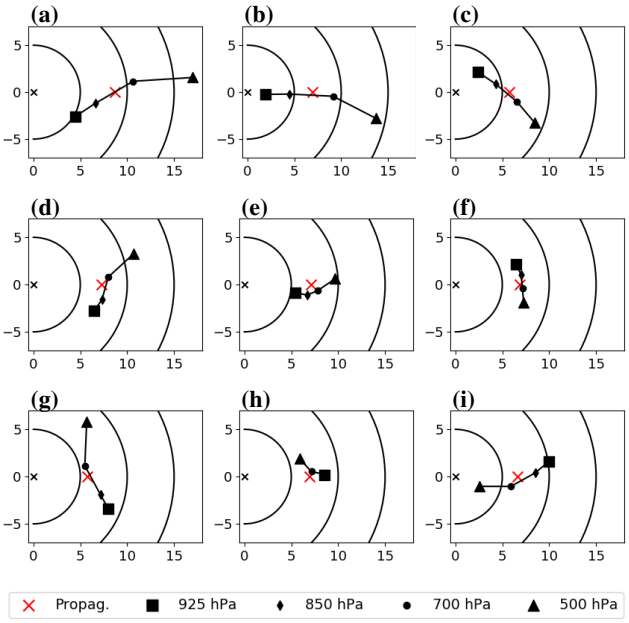

Figure 3. The mean hodographs associated with each SOM node displayed with the propagation direction towards the right. The square, diamond, circle, and triangle mark the SOM-mean, area-mean wind vector of the 925, 850, 700 and 500 hPa, respectively. The mean wind vectors are rotated with respect to the propagation vector of the polar low (red cross). Units on the x and y-axis are ms^{-1}. The origin is marked by a black "x" and black circular lines denote mean wind vectors with a strength of 5, 10 and 15 ms^{-1}.

These situations feature a strong horizontal temperature gradient. Genesis occurs most often in forward (node 1+2: 26%) and reverse shear (node 9: 24%), though also ~~right (~~node 3 (identified as right shear in the next section: 11%) and ~~left shear (~~node 7 (left shear: 14%) are common genesis situations. The SOM nodes associated with a low horizontal temperature contrast (5, 6 and 8) are predominantly lysis situations. Hence, PLs often evolve from nodes with stronger to nodes with weaker temperature gradients in the SOM matrix.

3.2 Connection to vertical wind shear

In ~~the forward-shear~~ nodes 1 and 2 ~~, the cold air is to the left of the propagation direction of the PL~~ the area-mean wind vector increases in the vertical from around 5 ms^{-1} at 925 hPa [1] to around 15 ms^{-1} at 500 hPa, both in propagation direction (Fig. ~~2), which is associated with a~~3a). This implies that the vertical-shear vector points in the direction of propagation of the system (Fig. 4)~~and thus an intensification of the area-mean wind vector with height~~ , which is similar to the area-vertical-mean wind vector (Fig. 3a)~~. The area-mean wind vector has a strength of more than 16 $^{-1}$ at 500 , but decreases to less than 5 $^{-1}$ at 925 (Fig. 3). Weak area-mean wind vectors indicate that the wind vectors cancel each other due to the closed cyclonic~~

[1] Note that weak area-mean wind vectors indicate that the wind vectors cancel each other due to an almost closed cyclonic circulation near the surface (Fig. 2).

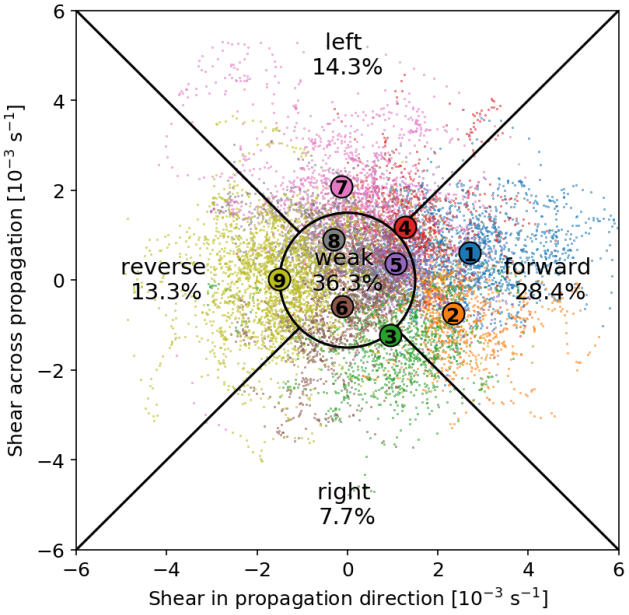

Figure 4. The categorisation along the vertical-shear vector (~~Equation~~Eq. 4). The mean value of the shear vector of all time steps associated with each node is marked by a coloured circle labelled with the number of the node. The shear vector of each individual polar-low time step is displayed as a small dot in the colour that represents the SOM node of the time step. The ~~mean value of the shear vector of all time steps associated with each node is marked by a thick dot. The~~ black circle and lines divide the shear-vector space into the categories ~~forward shear~~forward-shear, ~~right shear~~right-shear, ~~reverse shear~~reverse-shear, left-shear, ~~left shear~~ and ~~weak shear~~ weak-shear situations. The fraction of time steps associated with each category is displayed.

~~circulation near the surface~~ , hence the name forward shear. By thermal wind balance, a forward shear is associated with the cold air being on the left of the PL as seen from the direction of propagation (Fig. 2).

~~The reverse shear node~~Node 9 is the opposite to node 1 and 2 and features cold air to the right of the direction of propagation and thus a vertical-shear vector oriented opposite to the direction of propagation, reverse-shear conditions (Fig. 4). Reverse shear corresponds to a decrease of the strength of the mean wind vector with height, from 10 ms^{-1} at 925 hPa to 3 ms^{-1} at 500 hPa (Fig. 3i). This is consistent with Bond and Shapiro (1991) and Terpstra et al. (2016), who observed that reverse-shear systems are often accompanied by a strong low-level jet. Accordingly, reverse-shear conditions are characterised by an almost closed upper-level circulation and a strong near-surface trough (see Fig. 2).

The other two nodes with a strong vertical shear, node 3 and 7, have intermediate shear angles between forward and reverse conditions. PLs in node 3 are propagating towards colder air masses (Fig.2). The environmental flow of node 3 features warm-air advection associated with veering, a clockwise turning of the wind vector with height (Fig. 3c). The vertical wind shear is towards the right of the direction of propagation with an angle of 50±20° (Fig. 4) and hence node 3 is referred to as right-shear conditions.

Table 1. Definition of the vertical-shear categories as depicted in Figure 4.

Category	shear angle	shear strength
Forward	-45° to 45°	~~$> 1.5 \cdot 10^{-3}$~~ $\geq 1.5 \times 10^{-3}$ s^{-1}
Right	45° to 135°	~~$> 1.5 \cdot 10^{-3}$~~ $\geq 1.5 \times 10^{-3}$ s^{-1}
Reverse	135° to -135°	~~$> 1.5 \cdot 10^{-3}$~~ $\geq 1.5 \times 10^{-3}$ s^{-1}
Left	-135° to -45°	~~$> 1.5 \cdot 10^{-3}$~~ $\geq 1.5 \times 10^{-3}$ s^{-1}
Weak	all	~~$< 1.5 \cdot 10^{-3}$~~ $\leq 1.5 \times 10^{-3}$ s^{-1}

Node 7 is opposite to node 3, with PLs propagating towards warmer air masses featuring environmental cold-air advection associated with backing, an anti-clockwise rotation of the wind vector with height (Fig. 3g). The vertical wind shear is towards the left of the propagation direction at an angle of -90±30° (Fig. 4). Hence, node 7 is referred to as left-shear condition, where the geostrophic flow features an upper-level trough with its axis tilted perpendicular to the left of the low-level trough axis. The same is the case for node 3, but ~~the axis~~ here the axes are perpendicular in the opposite direction.

Node 4 represents an intermediate setup between node 1 and 7 with intermediate values in the shear angle (Fig. 4: -45± 20°). In the remaining nodes (5, 6 and 8) the vertical-shear strength is weak and hence the angle of the vertical shear is of less importance. The mean wind vectors of these nodes at different heights are almost uniform (Fig. 3) indicating that the flow is quasi-barotropically aligned (Fig. 2).

Given that the vertical-shear vector with respect to the propagation direction captures the different SOM nodes (Fig. 4) we suggest to use it as the key parameter to classify PLs as defined in Table 1. Sorting all PLs by their shear in propagation and cross-propagation direction, a continuous ~~spectrum~~ 2-dimensional parameter space emerges (Fig. 4). ~~While this implies that strict~~ The thresholds are to some degree arbitrary, ~~the choice of the exact thresholds was~~ but variations in the thresholds were found to have no qualitative influence on the following results.

Applying ~~a straight forward~~ the suggested sectioning of the parameter space (Fig 4), PLs in forward-shear ~~situations~~ environments generally occur more often (28.4%) than in reverse-shear situations (13.3%). Left-shear conditions (14.3%) are approximately as frequent as reverse shear conditions and right-shear situations are rather seldom (7.7%). In the following, these four categories are labelled as strong shear categories. In contrast, approximately 36.3% of the time steps have a weak shear of less than ~~$1.5 \cdot 10^{-3}$~~ $1.5 \times 10^{-3}\,s^{-1}$, which means that the wind vector is changing less than $1.5\,ms^{-1}$ per km altitude.

Note that this classification is based on individual PL time steps. In this way it is considered that the environmental shear often changes during the lifetime of an individual PL. The weak-shear class is the category with most time steps, however only 38 of the 374 PLs are within this class for their whole lifetime. In contrast, 189 PLs change between strong and weak shear during their development, mainly from strong to weak shear (Fig. 2). The shear angle varies by more than 90° during the lifetime for 80 of the 336 PLs that are featuring a strong shear. Hence, the shear strength and direction varies through the lifetime of an individual PL as its ambient environment changes.

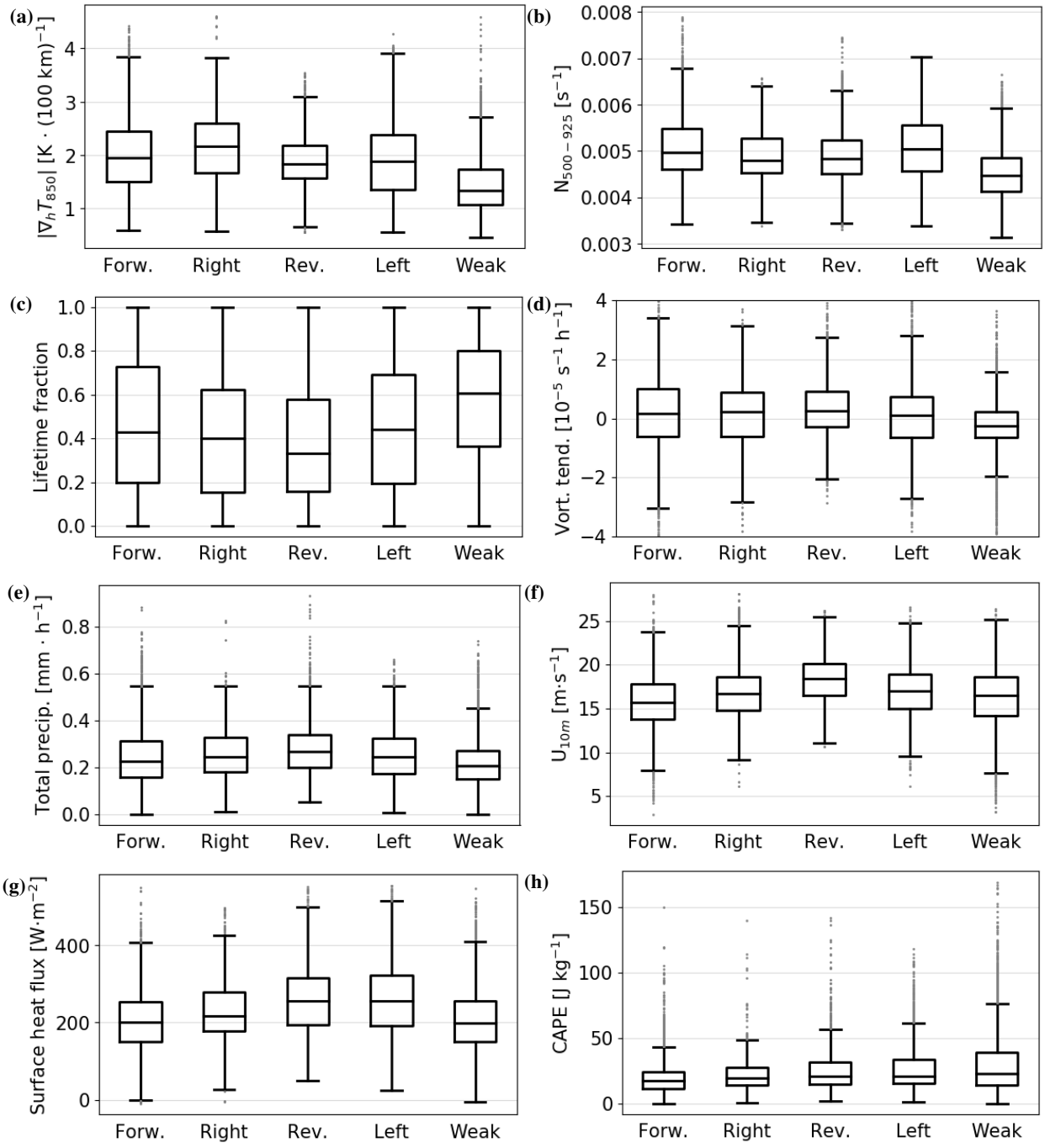

Figure 5. Distributions of different parameters for all time steps attributed to the shear categories introduced in Figure 4. The ~~mean~~ vorticity tendency is derived as described in Section 2.4. The lifetime fraction is given by the time step of a PL divided by its lifetime. For the other parameter, the mean value within a 250 km radius is calculated, except for the 10 m wind speed, where the maximum ~~value~~ is ~~used~~applied. For the computation of the mean static stability, total precipitation, surface heat fluxes, and CAPE, grid cells covered by land or sea-ice are excluded.

3.3 Characteristics of the shear categories

The ~~strength of~~ thermal wind relation associates the vertical wind shear ~~is related to the strength of~~ with the horizontal temperature gradient~~through the thermal wind. The strong shear~~ . This relation is evident for the environmental variables of the different shear categories. The strong-shear classes are exceeding a vertical wind shear of ~~$1.5 \cdot 10^{-3}$~~ $1.5 \times 10^{-3}\,\mathrm{s}^{-1}$ and have a median horizontal temperature gradient of around 2.0 K per 100 km (Fig. 5a). PLs within these categories thus most likely intensify through baroclinc instability. In contrast, the weak-shear category has a median temperature gradient of 1.3 K per 100 km and is thus considerably less baroclinic. While hurricane-like PLs might be feasible in this more symmetric category, there is little evidence for hurricane-like ~~PLs~~ intensification within this category.

Cyclogenesis of PLs in all shear categories is further supported by a low static stability ($N \approx 0.005\,\mathrm{s}^{-1}$, Fig. 5b)~~relative to typical synoptic-scale baroclinic environments (see Table 2). Low~~ , as a low static stability is associated with a ~~higher~~ high baroclinic growth rate (Vallis, 2017). The low static stability in ~~these PL environments implies~~ PL environments is often expressed by a high temperature contrast between the sea-surface and the upper troposphere~~associated with PLs, often expressed as~~ , SST-T_{500} (e.g. Zappa et al., 2014; Stoll et al., 2018; Bracegirdle and Gray, 2008).

The atmosphere is slightly less stable in reverse and right-shear situations (both median of $0.0048\,\mathrm{s}^{-1}$) than in forward and left-shear situations (both median of $0.0050\,\mathrm{s}^{-1}$). This was also pointed out by Terpstra et al. (2016), who found a larger temperature contrast between the sea surface and the 500 hPa level for reverse compared to forward-shear conditions. It ~~could~~ may be argued that the shear-strength threshold of ~~$1.5 \cdot 10^{-3}$~~ $1.5 \times 10^{-3}\,\mathrm{s}^{-1}$ should be lower for reverse and right-shear categories as a weaker vertical shear can be compensated by a lower static stability. We do not adapt such an adjustment, which would increase the fraction of reverse and right-shear conditions.

~~PL time steps with strong shear are~~ Strong shear is more common in the first half of the PL lifetime (Fig. 5c) and ~~are~~ more often associated with a positive vorticity tendency, depicting intensification (Fig. 5d)~~depicting intensification. PL time steps in the weak-shear category are predominantly occurring~~ . In contrast, weak shear is most common at later stages and associated with decay (70%). Even though some PL time steps in weak shear feature vortex intensification (30%), only for 6% of ~~these time steps are intensifying~~ the weak-shear time steps the vortex is rapidly intensifying in the local-mean relative vorticity at a rate of more than ~~$1 \cdot 10^{-5}$~~ $1 \times 10^{-5}\,\mathrm{s}^{-1}\,\mathrm{h}^{-1}$, whereas ~~for the high-shear categories on average~~ in strong-shear situations 22% of the time steps are ~~intensifying at such a~~ associated to a vortex intensification exceeding this rate. Closer investigation reveals that these 6% of intensifying time steps within the ~~weak shear~~ weak-shear category feature a shear close to the threshold separating between strong and ~~weak shear~~ weak-shear systems.

The static stability is considerably lower in the weak-shear category (median $N = 0.0044\,\mathrm{s}^{-1}$, Fig. 5b), which is most likely associated with this category appearing later during the PL ~~life time~~ lifetime when condensational latent-heat release has already destabilised the atmosphere.

~~While the~~ The area-mean total precipitation rate is $0.24\,\mathrm{mm\,h}^{-1}$ (median ~~), which~~ of all time steps) is rather low compared to extra-tropical cyclones~~, it~~ . The precipitation is somewhat stronger for reverse-shear conditions (Fig. 5e, ~~median~~ $0.27\,\mathrm{mm\,h}^{-1}$), which indicates that latent heat release by condensation is most important in this class, which may compen-

sate for a lower baroclinicity. In weak-shear condition, there is less precipitation (~~median~~ 0.21 $\mathrm{mmh^{-1}}$) than for the other categories, which is consistent with this class mainly containing the decaying stages of PLs. ~~It further indicates that~~ Moreover, extreme values in precipitation are lower for weak than for strong-shear situations (Fig. 5 dots), which contradicts the idea that convective processes are more important for the weak than the strong-shear class. Furthermore, the precipitation rates appear to be insufficient to represent intensification solely through convective processes~~is highly unlikely within this~~ , indicating that hurricane-like dynamics are unlikely in the weak-shear class.

The median in the area-maximum near-surface wind speed of ~~PLs is around~~ all PL time steps is 16.6 $\mathrm{ms^{-1}}$ ~~(median)~~. The near-surface winds are somewhat lower for forward (Fig. 5f, median ≈15.7 $\mathrm{ms^{-1}}$) and higher for reverse-shear conditions (median ≈18.4 $\mathrm{ms^{-1}}$), which is consistent with Michel et al. (2018), who found that reverse-shear polar mesoscale cyclones (PMCs) have on average a stronger lifetime-maximum near-surface wind speed (22 $\mathrm{ms^{-1}}$) than forward-shear PMCs (19 $\mathrm{ms^{-1}}$). Hence, PL detection with a criteria on the near-surface wind speed, as suggested in the definition by Rasmussen and Turner (2003) with 15 $\mathrm{ms^{-1}}$, excludes more forward than reverse-shear systems.

In reverse-shear conditions, the environmental flow is strongest at low levels and decreases with height (~~node 9 in Fig. 2,~~ 3j), which is consistent with Terpstra et al. (2016). For forward-shear conditions, the environmental-mean wind vector is weak at low levels (Fig. 3~~) and hence~~ a) and the near-surface wind is mainly associated with the cyclonic circulation of the PL (see also Fig. 2).

The area-mean turbulent heat fluxes at the surface are highest for left and reverse-shear conditions (median 257 and 256 $\mathrm{Wm^{-2}}$, respectively, Fig. 5g) and slightly lower for right, forward, and weak-shear conditions (median 216, 201 and 200 $\mathrm{Wm^{-2}}$, respectively). Higher surface turbulent heat fluxes for reverse-shear conditions were also found by Terpstra et al. (2016) and associated with the stronger near-surface winds. The higher turbulent fluxes in left-shear conditions ~~is~~ are most likely connected to the large-scale flow being associated with ~~cold air~~ cold-air advection (SOM node 7 in Fig. 2). In the weak-shear category, surface fluxes are not exceptionally high, rendering it unlikely that the WISHE mechanism is ~~active for these PLs~~more relevant for this category than for the strong-shear categories. However, also for the strong-shear categories surface fluxes appear to have a limited direct effects on the PL intensification (Sec. 4.2), questioning the relevance of the WISHE mechanism as being of primary importance for PL development.

All shear categories feature low values in the convective available potential energy (CAPE, Fig. 5h), with median values around 20 $\mathrm{Jkg^{-1}}$ and only a few PL time steps with CAPE above 50 $\mathrm{Jkg^{-1}}$. This is in accordance with Linders and Saetra (2010), who found that CAPE is consumed instantaneously during PL development as it is produced. In order to be of dynamic relevance, CAPE values would need to be at least one order of ~~significantly~~ magnitude larger (Markowski and Richardson, 2011). Hence the CISK mechanism that relies on CAPE appears unlikely to explain intensification of PLs in the STARS dataset.

3.4 Cloud morphology

Strong-shear conditions most commonly feature comma-shaped clouds (53% of the labelled time steps by Rojo et al. (2019)), whereas spirali-form clouds are less frequent in these categories (30%, Fig. 6). Weak-shear conditions, on the other hand,

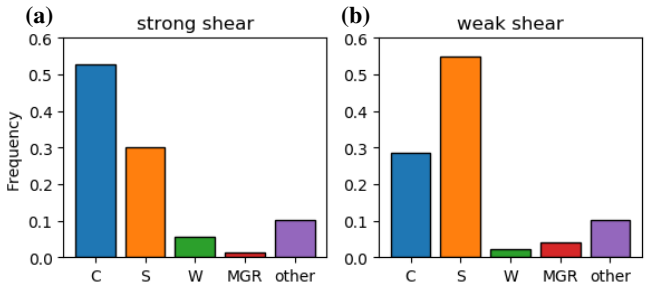

Figure 6. Occurrence of the cloud morphologies introduced by Rojo et al. (2019) ~~within~~ for the time steps with a strong (left) and weak (right) vertical shear. The cloud morphologies are: C = comma shaped, S = spirali form, W = wave system, MGR = merry-go-round.

feature mainly spirali-form clouds (55%) and less frequently comma clouds (29%). This is consistent with the findings of Yanase and Niino (2007) that the cloud structure is connected to the baroclincity of the environment.

However, we find little evidence for axis-symmetric intensification in an environment with weak shear. Accordingly, the axis-symmetric, spirali-form system simulated by Yanase and Niino (2007) had a considerably lower growth rate than the systems within a baroclinic environment (their Fig. 3). Instead, we find that time steps in the weak-shear category resemble the occlusion stage of a baroclinic development (Fig. 2) with a quasi-barotropic alignment of the flow (Fig. 3). The spirali-form cloud signature may be explained by a baroclinic development with a warm seclusion, as suggested by the Shapiro-Keyser model (Shapiro and Keyser, 1990). In later stages, this model resembles a spirali-form cloud signature. We therefore propose the warm seclusion pathway as an alternative hypothesis for the formation of ~~hurricane-like PLs~~ PLs that appear hurricane-like.

The frequency of wave-type clouds (Rojo et al., 2015) is higher within the ~~strong shear~~ strong-shear (6%) than the weak-shear category (2%). Similar to ~~comma-clouds~~comma clouds, wave-type clouds are often associated with a baroclinic development (Rasmussen and Turner, 2003). The frequency of merry-go-round systems is higher within the weak shear (4%) compared to the strong-shear categories (1%). Merry-go-round are often associated with an upper-level cold cut-off low in the absence of considerable baroclinicity (Rasmussen and Turner, 2003).

3.5 Synoptic conditions associated with the shear categories

Within the Nordic Seas, each of the shear categories is associated with a distinct synoptic-scale situation (Fig. 7)~~. PLs in forward-shear conditions typically form when~~ , leading to typical locations and propagation directions of PLs within each shear category. Forward-shear conditions often form south or south-west of a synoptic-scale ~~low-pressure systemis~~ low-pressure system, located in the ~~north-eastern Barents Sea causing a marine cold-air outbreak around Svalbard~~ northern Barents Sea (Fig. 7a). ~~Most PLs within this category occur south of Svalbard and feature an eastwardpropagation~~The synoptic low causes a marine cold-air outbreak on its western side and a zonal flow further downstream on its southern side almost along the isotherms. Forward-shear PLs most frequently occur in this zonal flow and consequently propagate eastward.

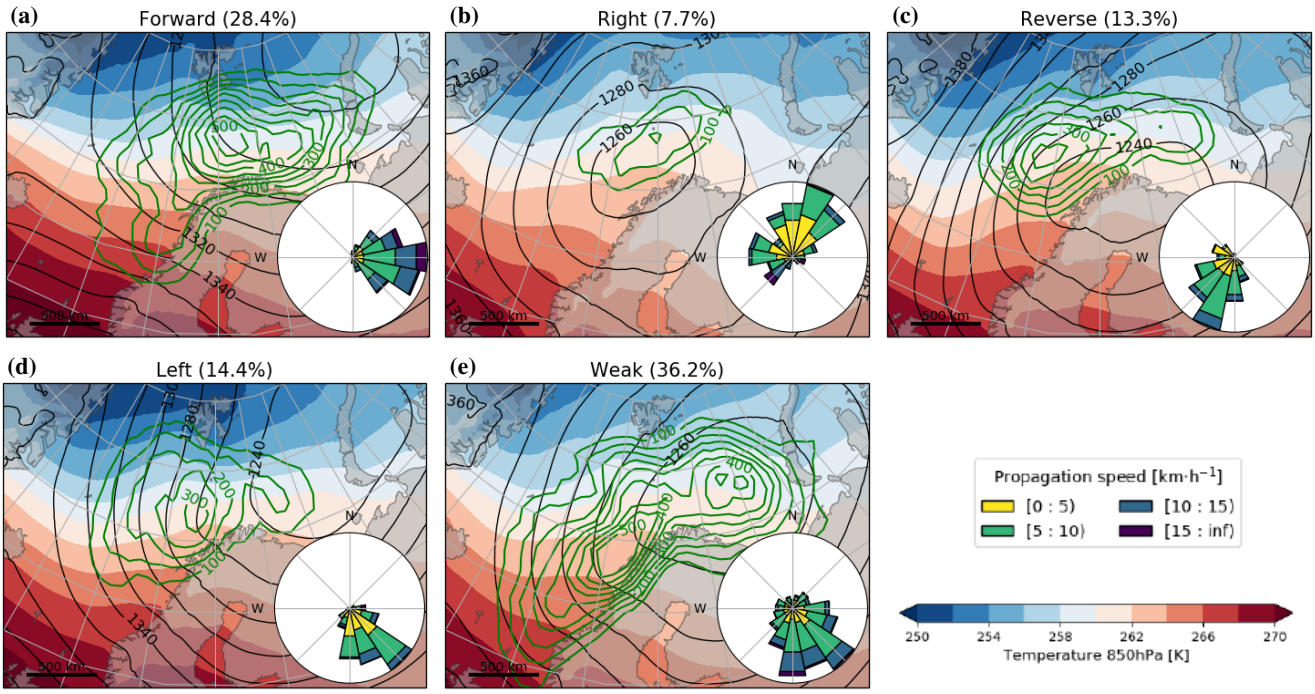

Figure 7. Composite maps of the 850 hPa temperature (shading) and geopotential height (black contours) associated with the polar lows within each shear category. Green contours: ~~Track~~ track densities associated with each category calculated by the number of track points within a 250 km radius. The roses depict the track distribution of the propagation direction and speed.

The synoptic-scale situation for reverse-shear PLs mainly features a low-pressure system over northern Scandinavia leading to a cold-air outbreak ~~to the west of Svalbard~~ from the Arctic to the Norwegian Sea, where most reverse-shear PLs develop (Fig. 7c). ~~In the Norwegian Sea, where most~~ The flow in which reverse-shear PLs ~~develop, the flow~~ typically occur is south-westward, consistent with their direction of propagation almost along the isotherms, though with the cold side on the opposite side as seen from the direction of propagation of ~~these~~ forward-shear PLs. The ~~typical~~ most frequent location and propagation ~~directions~~ direction of forward and reverse-shear ~~PL~~ PLs is in accordance with ~~(Terpstra et al., 2016; Michel et al., 2018)~~ Terpstra et al. (2016) and Michel et al. (2018).

In left-shear conditions, a low pressure system is located over the Barents Sea causing a ~~south-~~ south to south-eastward ~~flow~~ directed cold-air outbreak across the isotherms towards a warmer environment (Fig. 7~~c).~~ d). Hence, left-shear PLs primarily occur ~~to the~~ south of Svalbard at the leading edge of the cold-air outbreak. Right-shear PLs predominantly occur to the east and north-east of a synoptic-scale low located in the Norwegian Sea (Fig. 7~~d~~b). In this situation, PLs propagate ~~north-~~ north and westward into colder air masses.

Weak-shear conditions are more variable than the other categories (Fig. 7e). PLs occur most frequently in more southerly locations near the coast of Norway and in the eastern Barents Sea, corresponding to lysis locations. A separation of the weak-shear conditions for different areas (not shown) reveals that they primarily occur downstream of one of the strong-

shear categories within an area of low temperature contrast. The latter is consistent with this category mainly being associated with PLs in mature and decaying ~~PLs~~ stages that originated from one of the other categories.

4 Intensification mechanisms

4.1 Baroclinic setup

The temperature as well as the upper and lower-level flow field for forward-shear PLs (Fig. 8a) ~~resembles~~ resemble the structure of a smaller version of a mid-latitude baroclinic cyclone that develops along the polar front featuring a typical up-shear[2] tilt with height of the low-pressure anomaly (e.g. Dacre et al., 2012), where the trough axis of the tropopause depression is displaced against the shear vector compared to the closed surface-pressure circulation. Reverse-shear systems, are characterised by an intense low-level trough together with a tropopause trough that is centred up-shear (Fig. 8g).

Right and left-shear conditions are characterised by a closed low-level vortex or a low-level trough, respectively, and feature a tropopause depression with its trough axis located up-shear (Fig. 8d,j). Thus, all strong-shear categories feature an up-shear vertical tilt between the surface pressure anomaly and the upper-level depression, which is characteristic for baroclinic development (Holton and Hakim, 2013).

Consistent with the vertical tilt of the pressure anomaly, the low-level circulation is associated with down-gradient warm-air advection down-shear in the warm sector. For forward (reverse) shear conditions, the warm sector is ahead of (behind) the PL with respect to its propagation direction. For right (left) conditions, the warm sector lies to the right (left) side of the PL track. Analogously, the low-level circulation is associated with an up-gradient cold-air advection in the cold sector, which is located up-shear. Low-level temperature advection by the cyclone generates eddy available potential energy and contributes to the amplification of the PL (see first term of equation 5 in Terpstra et al. (2015)).

~~The~~ Downstream of the upper-level trough ~~is associated with ascent at its leading edge (Supplementary Figure~~the flow is diverging and hereby forcing mid-level ascent (Supplementary Fig. 11)~~located near the surface pressure anomaly and hence leads to a further intensification of the PL through vorticity stretching. The ascending air~~ , which is co-located to the area of precipitation (second column in Fig. 8). The ~~ascent occurs in an area that is close to conditional instability ($\theta_{e,2m} - \theta_{e,500hPa} \approx -6\,K$, Supplementary Figure 11).~~

rising motion occurs near the surface low pressure anomaly and further intensifies the PL through vortex stretching and tilting (not shown). The interaction between the upper and lower levels is ~~further~~ supported by a low ~~vertical stability up to the tropopause at around 400~~ static stability between lower and upper tropospheric levels (Fig. 5d). This suggests that the baroclinic development spans the entire depth of the troposphere and is not confined to the low levels as suggested by Mansfield (1974).

[2] opposite direction to the shear vector

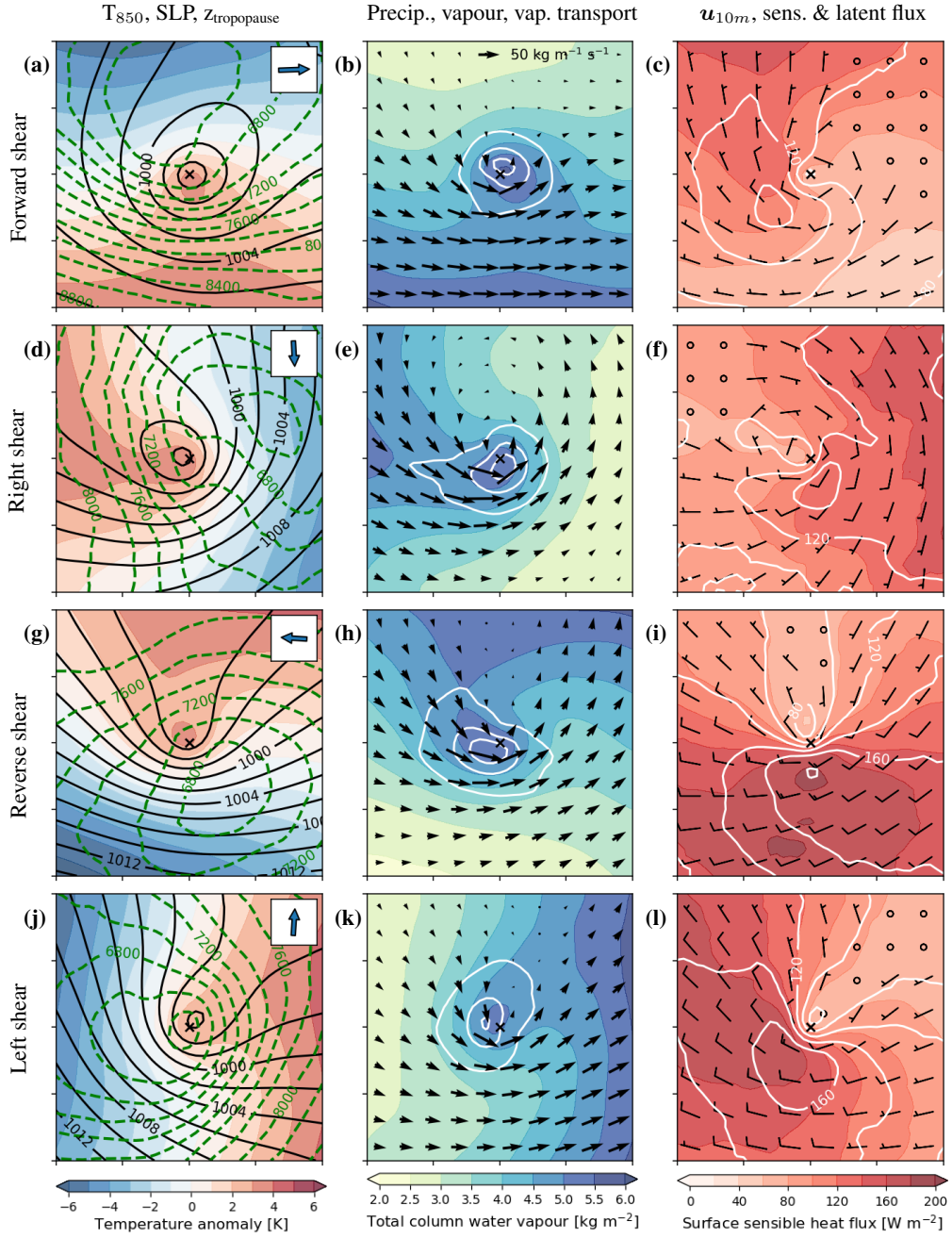

Figure 8. Composite maps ~~in~~ on a PL-centred grid with propagation direction towards the right associated with four strong-shear categories. Left column: temperature anomaly at 850 hPa (shading), sea-level pressure (black contours, 2 hPa spacing), and tropopause height (green-dashed contours, spacing 200 m). The inset shows the mean of the vertical-shear vector within the category (compare to Fig. 4). Middle column: ~~Total~~ total column water vapour (shading), total precipitation (contours, 0.2 mmh^{-1} spacing), and vertically integrated water vapour flux (arrow, reference vector at top). Right column: 10 m wind vectors (quivers), surface sensible heat flux (shading) and surface latent heat flux (contours, spacing 20 Wm^{-2}).

4.2 Diabatic contribution

Most of the precipitation occurs along the warm front in the sector left down-shear of the PL centre (Fig. 8~~), which is also the location of the~~ b,e,h,k) in an area of low conditional stability ($\theta_{e,2m} - \theta_{e,500hPa} \approx -6\,K$, Supplementary Fig. 11), likely moist symmetrically neutral or slightly unstable (Kuo et al., 1991b; Markowski and Richardson, 2011). The area of precipitation is co-located with increased cloud cover featuring a ~~comma-shaped form~~ comma shape (Fig. 2). The release of latent heat associated with the precipitation leads to the production of potential vorticity underneath the level of strongest heating and hence intensifies the low-level circulation within a moist-baroclinic framework (Davis and Emanuel, 1991; Stoelinga, 1996; Kuo et al., 1991b; Bala . As the latent heat release primarily occurs in the warm sector, it further increases the horizontal temperature gradient, which contributes to the generation of eddy available potential energy (Terpstra et al., 2015).

For all shear conditions, the moisture that is converted to precipitation originates from the warm sector. In forward and left-shear conditions, PLs are propagating towards the warm and moist sector (Fig. 8b,k), while the moisture is transported into the area of precipitation from the rear of the PL in reverse and right-shear conditions. The comma-cloud and area of main precipitation appears to be associated with the warm conveyor belt, since the trajectories that contribute to the precipitation origin in the warm sector, feature the strong ascent rates (Supplement Fig. 11) and ascent up on the warm front.

The highest sensible heat fluxes occur on the cold side of the PL (Fig. 8c,f,i,l), leading to a reduction of low-level baroclinicity and a diabatic loss of eddy available potential energy. Latent heat fluxes are roughly co-located with the sensible heat fluxes, but occur further downstream where the air mass is already warmer and has therefore a higher capacity for holding water vapour. As the ~~highest~~ largest latent heat fluxes occur in the cold sector, the moisture released there would need to be advected around the PL to contribute to the diabatic intensification in the warm sector. Therefore, the ~~latent heat flux appears~~ area with maximum latent heat fluxes appear to have a limited direct effect on the intensification of the PL. ~~However, the~~ The latent heat fluxes in the warm sector yield an additional source of moisture that can more directly contribute to intensify the precipitation.

The ~~distribution of the heat fluxes does, however , not contradict that~~ surface heat fluxes appear to have a limited contribution, however the fluxes are important in creating an environment conducive for PL development (Kuo et al., 1991a; Haualand and Spengler, 202 . Sensible heat fluxes prior and during the PL development create an environment of low static stability, which supports the baroclinic intensification. ~~Even though the highest latent heat fluxes are displaced from the warm sector, the~~ The polar air mass in which ~~the PL develops benefits from the surface evaporation that fuels the~~ PLs develop typically origins from sea-ice or land-covered regions (Fig. 7) and would be very dry without surface evaporation occurring on the fetch prior the PL development. A diabatic contribution from latent heat release appears to be required in order to explain the rapid intensification of PLs (Section 4.3).

4.3 Scale considerations

Given the dry-baroclinic growth rate $\sigma_{max} = 0.3 \frac{f}{N} \frac{\partial \boldsymbol{u_s}}{\partial z}$ and diameter of the most unstable mode $d_\sigma \approx 2 \frac{NH}{f}$ ~~(e.g. p.354ff Vallis, 2017)~~ (e.g. Vallis, 2017, p.354ff), inserting typical values for PLs results in $\sigma_{max} \approx 1.5\,\mathrm{day}^{-1}$ and $d_\sigma \approx 500\,\mathrm{km}$ (Table 2), where the growth rate is close to ~~observed PLs (≈~~the observed median value of the PLs investigated in this study ($1.8\,\mathrm{day}^{-1}$, Fig.9a).

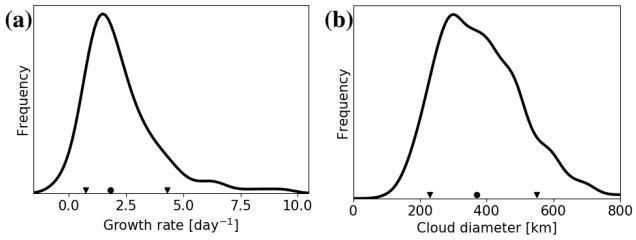

Figure 9. (a) Distribution of the ~~lifetime-maximum in the growth rate of~~ growth-rate maximum during the PL lifetime. (b~~, c~~) Distribution of the cloud diameter for all PL time steps ~~based on the cloud diameter~~ according to Rojo et al. (2019). The dot denotes the median, and the triangles the 10th and 90th percentiles of the distributions. The curves are computed with a Gaussian kernel.

Table 2. Approximation of values required for the determination of the growth rate, σ_{max}, and the diameter, d_σ, of the fastest growing mode by dry-baroclinic theory. For PLs, the static stability, N, is obtained from Figure 5, the shear strength, $\frac{\partial u_s}{\partial z}$, from Figure 4, and the tropopause level, H, from Figure 8. The Coriolis parameter, f, is computed for 70°and 45°latitude for PLs and mid-latitude cyclones, respectively. For mid-latitude cyclones N, $\frac{\partial u_s}{\partial z}$ and H are approximated with the use of values from Figure 2b, 3h and 3i, respectively, of Stoll et al. (2018).

	N [s^{-1}]	$\frac{\partial u_s}{\partial z}$ [s^{-1}]	H [m]	f [s^{-1}]	σ_{max} [day^{-1}]	d_σ [km]
Polar lows	0.005	~~$2 \cdot 10^{-3}$~~ 2×10^{-3}	7,000	1.4 ~~$\cdot 10^{-4}$~~ $\times 10^{-4}$	1.5	500
Mid-latitude cyclones	0.012	~~$3 \cdot 10^{-3}$~~ 3×10^{-3}	9,000	1.0 ~~$\cdot 10^{-4}$~~ $\times 10^{-4}$	0.6	2,400

These values are quite different to typical mid-latitude cyclones, with $\sigma_{max} \approx 0.6\,\mathrm{day}^{-1}$ and $d_\sigma \approx 2400\,\mathrm{km}$ (Table 2), where the largest contribution to the faster growth and smaller scale of PLs appears to be due to the reduced static stability for PLs ($N \approx 0.005\,\mathrm{s}^{-1}$) compared to mid-latitude cyclones ($N \approx 0.012\,\mathrm{s}^{-1}$). The larger Coriolis parameter, f, and lower tropospheric depth, H, contribute only to a smaller extent to faster PL intensification and the vertical-shear, $\frac{\partial u_s}{\partial z}$, is actually weaker for PLs compared to mid-latitude cyclones.

The estimation of the size of PLs is challenging. Often the diameter of the cloud associated with the PL is utilised for this purpose (e.g. Rojo et al., 2015), where the typical cloud diameter based on Rojo et al. (2019) is around 370 km (median, Fig. 9b). The cloud size estimated for the medium-level comma-shaped clouds of SOM 1, 3, 7 and 9 in Figure 2 is around 400 km. The vertical tilt between the upper and lower-level pressure disturbance (Fig. 8a,d,g), which in dry-baroclinic theory is a quarter of the wavelength of the fastest growing mode, is approximately 200 km, confirming the estimated diameter of around 400 km. Hence, the observed diameters are close to the theoretical ~~estimates~~estimate of 500 km.

The slight discrepancies between observation and theory are most likely attributable to latent heat release, which is observed for all shear configurations (Fig. 8b,e,h,k). The release of latent heat increases the growth rate and reduces the diameter of the fastest growing mode ~~(Sardie and Warner, 1983; Yanase and Niino, 2007; Terpstra et al., 2015)~~(Sardie and Warner, 1983; Kuo et al., 1991
. Moist-baroclinic instability therefore appears to be the most plausible intensification mechanism for PLs, which was also proposed by Terpstra et al. (2015) and Haualand and Spengler (2020).

5 Discussion and conclusion

We applied the SOM algorithm to ~~the 850 temperature anomaly field to~~ identify archetypal meteorological configurations of PL environments (Fig. 2). The ~~application of the algorithm to other atmospheric fields, such as the temperature anomaly at different height levels, specific humidity, and upper or lower-level geopotential height anomaly reveal similar results, which demonstrates the generality of our results.~~

~~The different nodes in~~ different nodes in the SOM matrix display that PLs occur in environments of thermal contrast of variable strength, where the temperature gradient may take any orientation compared to the propagation direction of the system. The variability among PLs in other variables projects well on the SOM nodes (Supplement section 3).

The classification obtained from the SOM matrix can be ~~categorised by~~ reduced to one single variable, the vertical-shear vector with respect to the propagation direction (Fig. 4)~~. We used~~ , which we use to separate PLs into five classes. We define a threshold of 1.5 ~~$\cdot 10^{-4}$~~ $\times 10^{-3}\,\mathrm{s}^{-1}$ ~~to classify~~ in the vertical-shear ~~vector into strong directional shear categories above this threshold and~~ strength to distinguish between weak-shear ~~conditions below.Our~~ and strong-shear situations.

Weak-shear conditions are predominantly associated with spirali-form clouds, whereas strong-shear situations with comma-shaped clouds (Fig. 6). However, weak-shear situations occur mainly at the end of the PL lifetime and are mainly associated with decaying PL stages. In contrast, PL intensification predominantly occurs in environments with a strong vertical shear.

To identify the PL dynamics, the strong-shear situations are further separated by the vertical-shear angle into four classes. Hereby, our analysis confirms the usefulness of the classification suggested by Duncan (1978) into forward and reverse-shear PLs with the vertical-shear vector in the same or opposite direction of the PL propagation, respectively. In addition to the previously identified shear categories, we find PL configurations that feature a shear vector directed to the left or right with respect to the propagation of the PLs, which we refer to as left or right-shear conditions, respectively.

Forward-shear PLs occur predominantly in an eastward flow in the Barents Sea with cold air to the left of the direction of propagation (Fig. 7a). Reverse-shear PLs mainly develop in the Norwegian Sea in a southward flow with cold air on the right-hand side. Left-shear PLs occur at the leading edge of ~~cold air~~ cold-air outbreaks and propagate towards a warmer environment, while right-shear PLs propagate towards a colder environment and occur when warmer air is advected towards a polar air mass. The shear situation of an individual PL can, however, change during its lifetime.

The baroclinic structure of the four strong shear categories features a vertical tilt between the surface and upper-level pressure anomaly against the vertical-shear vector (Fig. 8). The upper-level anomaly is captured by a tropopause depression, indicating that ~~PL~~ PLs span the entire depth of the polar troposphere. The atmospheric configuration features the classic growth through baroclinic instability, where the anomalies are organised by the vertical-shear vector. Therefore, the classification of PLs based on their environmental thermal fields successfully reveals the dominant development mechanism.

~~Weak-shear conditions are predominantly associated with spirali-form clouds, whereas strong-shear situations with comma-shaped clouds (Fig. 6). However, weak-shear situations occur mainly at the end of the PL lifetime and are seldomly associated with a considerable intensification.~~ Consistent with the cloud structure, precipitation mainly develops along the warm front, which is

located in the sector between the direction of the vertical-shear vector and its left side. Hence, the orientation of the comma cloud is determined by the shear vector.

The arrangement of the baroclinic structure in conjunction with the location of the latent heat release suggests a mutual interaction between the two. Latent heating enhances the baroclinicity and the diabatically-induced ascent is in phase with the baroclinically-forced adiabatic vertical motion. Thus, the effect of latent heat release is not only a linear addition to the dry-baroclinic dynamics, but also interacts directly with the adiabatic dynamics in a moist-baroclinic framework (Kuo et al., 1991b) .

The surface latent heat fluxes appear to be only indirectly relevant, as the maxima in the latent heat flux are significantly displaced from the precipitation (Fig. 8). Instead, most moisture converges from the warm and moist side of the PL, as was previously observed by ~~Terpstra et al. (2015); Stoll et al. (2020)~~Terpstra et al. (2015) and Stoll et al. (2020). The direct effect of surface sensible heat fluxes would act to reduce the environmental temperature gradient and thereby most likely contributes to a dampening of the development. However, surface fluxes also shape the environment in which the PLs develop, where polar air masses would be relatively dry without experiencing significant latent heat fluxes. The sensible heat flux reduces the static stability, which is also conducive for baroclinic development.

Applying dry-baroclinic theory to atmospheric values for PL environments yields growth rates and diameters that are comparable to ~~observed~~ the observed values for PLs, where the discrepancies can most likely be attributed to latent heat release, which enhances growth and reduces the scale ~~(e.g., Sardie and Warner, 1983; Terpstra et al., 2015; Haualand and Spengler, 2020)~~(e.g. Sardie and . We therefore suggest that moist-baroclinc development is the dominant mechanism leading to the intensification of the majority of PLs. The considerably higher growth rates and smaller disturbance scale of PLs as compared to mid-latitude cyclones appear to be primarily associated with a lower static stability and to a ~~lesser~~ smaller extent to a higher Coriolis parameter and a lower tropopause height. The lower stability is associated with the ~~moist-adiabatic~~ lapse rate in ~~cold air outbreaks~~ cold-air outbreaks being moist adiabatic (Linders and Saetra, 2010), which, due to the low temperatures of polar air masses, is nearly equivalent to the dry adiabat.

Generally our analysis based on ERA-5 provides no evidence for the ~~existence~~ occurrence of hurricane-like ~~PLs that intensifies mainly by latent heat release.~~ intensification of PLs predominantly by convective processes within an environment of low vertical shear. This casts doubt on the PL spectrum ranging from comma-shaped, baroclinic systems to spirali-form, hurricane-like types. Instead, most PLs intensify in a baroclinic environment characterised by a strong vertical shear. However, PLs often develop a warm core (e.g. Bond and Shapiro, 1991; Nordeng and Rasmussen, 1992; Føre et al., 2011), which is typical for baroclinic development following the Shapiro-Keyser model with a warm seclusion and a spirali-form cloud structure at the later stages of the life cycle (Shapiro and Keyser, 1990). Hence, we hypothesise that PLs with spirali-form clouds are ~~most likely~~ best described as secluded cyclones, as was argued for previously (Hewson et al., 2000). To further clarify this hypothesis, studies using high-resolution datasets, such as CARA (CAR), should be used to investigate the frontal ~~lifecycle~~ life-cycle in PLs.

Data availability. The tracks of the ERA-5 matched STARS PLs are provided.

Author contributions. PS designed the study and performed the analysis. All authors contributed to the discussion of the methods and results. PS wrote the manuscript with contributions from all authors.

Competing interests. The authors declare no competing interests.

Acknowledgements. We thank ECMWF for providing access to data from the ERA-5 reanalysis. Parts of the data were processed at the supercomputer Stallo provided by the Norwegian Metacenter for Computational Science (NOTUR) under the project NN9348K. We ~~also thank Denis Sergeevfor providing~~ were supported by Denis Sergeev, who provided access and support to the PMC-tracking algorithm and by Tiina Nygård~~for sharing~~ , who shared code for the application of the SOM algorithm. Four anonymous reviewers are also thanked for their critical questions, which improved the manuscript.

References

Copernicus Arctic Regional Reanalysis Service, https://climate.copernicus.eu/copernicus-arctic-regional-reanalysis-service, accessed: 2020-06-11.

Balasubramanian, G. and Yau, M.: The life cycle of a simulated marine cyclone: Energetics and PV diagnostics, Journal of the atmospheric sciences, 53, 639–653, 1996.

Bond, N. A. and Shapiro, M.: Polar lows over the Gulf of Alaska in conditions of reverse shear, Monthly weather review, 119, 551–572, 1991.

Bracegirdle, T. J. and Gray, S. L.: An objective climatology of the dynamical forcing of polar lows in the Nordic seas, International Journal of Climatology, 28, 1903–1919, 2008.

Businger, S. and Reed, R. J.: Cyclogenesis in cold air masses, Weather and Forecasting, 4, 133–156, 1989.

Charney, J. G. and Eliassen, A.: On the growth of the hurricane depression, Journal of the Atmospheric Sciences, 21, 68–75, 1964.

Claud, C., Heinemann, G., Raustein, E., and McMurdie, L.: Polar low le Cygne: satellite observations and numerical simulations, Quarterly Journal of the Royal Meteorological Society, 130, 1075–1102, 2004.

Dacre, H., Hawcroft, M., Stringer, M., and Hodges, K.: An extratropical cyclone atlas: A tool for illustrating cyclone structure and evolution characteristics, Bulletin of the American Meteorological Society, 93, 1497–1502, 2012.

Davis, C. A. and Emanuel, K. A.: Potential vorticity diagnostics of cyclogenesis, Monthly weather review, 119, 1929–1953, 1991.

De Boor, C.: A practical guide to splines, Springer Verlag, 1978.

Duncan, C.: Baroclinic instability in a reversed shear-flow, Meteorological Magazine, 107, 17, 1978.

Emanuel, K. A.: An air-sea interaction theory for tropical cyclones. Part I: Steady-state maintenance, Journal of the Atmospheric Sciences, 43, 585–605, 1986.

Emanuel, K. A. and Rotunno, R.: Polar lows as arctic hurricanes, Tellus A, 41, 1–17, 1989.

Forbes, G. S. and Lottes, W. D.: Classification of mesoscale vortices in polar airstreams and the influence of the large-scale environment on their evolutions, Tellus A: Dynamic Meteorology and Oceanography, 37, 132–155, 1985.

Føre, I., Kristjánsson, J. E., Saetra, Ø., Breivik, Ø., Røsting, B., and Shapiro, M.: The full life cycle of a polar low over the Norwegian Sea observed by three research aircraft flights, Quarterly Journal of the Royal Meteorological Society, 137, 1659–1673, 2011.

Føre, I., Kristjánsson, J. E., Kolstad, E. W., Bracegirdle, T. J., Saetra, Ø., and Røsting, B.: A 'hurricane-like'polar low fuelled by sensible heat flux: high-resolution numerical simulations, Quarterly Journal of the Royal Meteorological Society, 138, 1308–1324, 2012.

Harrold, T. and Browning, K.: The polar low as a baroclinic disturbance, Quarterly Journal of the Royal Meteorological Society, 95, 710–723, 1969.

Haualand, K. F. and Spengler, T.: Direct and Indirect Effects of Surface Fluxes on Moist Baroclinic Development in an Idealized Framework, Journal of the Atmospheric Sciences, pp. 1–43, 2020.

Hersbach, H. and Dee, D.: ERA5 reanalysis is in production, ECMWF newsletter, 147, 5–6, 2016.

Hewson, T., Craig, G., and Claud, C.: Evolution and mesoscale structure of a polar low outbreak, Quarterly Journal of the Royal Meteorological Society, 126, 1031–1063, 2000.

Holton, J. and Hakim, G.: An Introduction to Dynamic Meteorology, vol. 5 of *Academic Press*, Elsevier Science, 2013.

Jonassen, M. O., Chechin, D., Karpechko, A., Lüpkes, C., Spengler, T., Tepstra, A., Vihma, T., and Zhang, X.: Dynamical processes in the Arctic atmosphere, in: Physics and Chemistry of the Arctic Atmosphere, pp. 1–51, Springer, 2020.

Kohonen, T.: Self-organizing maps, Berlin: Springer, 3rd edn., 2001.

Kolstad, E. W. and Bracegirdle, T.: Sensitivity of an apparently hurricane-like polar low to sea-surface temperature, Quarterly Journal of the Royal Meteorological Society, 143, 966–973, 2017.

Kolstad, E. W., Bracegirdle, T. J., and Zahn, M.: Re-examining the roles of surface heat flux and latent heat release in a "hurricane-like" polar low over the Barents Sea, Journal of Geophysical Research: Atmospheres, 121, 7853–7867, 2016.

Kristjánsson, J. E., Barstad, I., Aspelien, T., Føre, I., Godøy, Ø., Hov, Ø., Irvine, E., Iversen, T., Kolstad, E., Nordeng, T., et al.: The Norwegian IPY–THORPEX: Polar lows and Arctic fronts during the 2008 Andøya campaign, Bulletin of the American Meteorological Society, 92, 1443–1466, 2011.

Kuo, Y.-H., Low-Nam, S., and Reed, R. J.: Effects of surface energy fluxes during the early development and rapid intensification stages of seven explosive cyclones in the western Atlantic, Monthly Weather Review, 119, 457–476, 1991a.

Kuo, Y.-H., Shapiro, M., and Donall, E. G.: The interaction between baroclinic and diabatic processes in a numerical simulation of a rapidly intensifying extratropical marine cyclone, Monthly Weather Review, 119, 368–384, 1991b.

Laffineur, T., Claud, C., Chaboureau, J.-P., and Noer, G.: Polar lows over the Nordic Seas: Improved representation in ERA-Interim compared to ERA-40 and the impact on downscaled simulations, Monthly Weather Review, 142, 2271–2289, 2014.

Linders, T. and Saetra, Ø.: Can CAPE maintain polar lows?, Journal of the atmospheric sciences, 67, 2559–2571, 2010.

Mansfield, D.: Polar lows: The development of baroclinic disturbances in cold air outbreaks, Quarterly Journal of the Royal Meteorological Society, 100, 541–554, 1974.

Markowski, P. and Richardson, Y.: Mesoscale meteorology in midlatitudes, vol. 2, John Wiley & Sons, 2011.

Michel, C., Terpstra, A., and Spengler, T.: Polar Mesoscale Cyclone Climatology for the Nordic Seas Based on ERA-Interim, Journal of Climate, 31, 2511–2532, 2018.

Noer, G. and Lien, T.: Dates and Positions of Polar lows over the Nordic Seas between 2000 and 2010, Met. no report, 16, 2010, 2010.

Nordeng, T. E. and Rasmussen, E. A.: A most beautiful polar low. A case study of a polar low development in the Bear Island region, Tellus A, 44, 1992.

Nygård, T., Graversen, R. G., Uotila, P., Naakka, T., and Vihma, T.: Strong dependence of wintertime Arctic moisture and cloud distributions on atmospheric large-scale circulation, Journal of Climate, 32, 8771–8790, 2019.

Ooyama, K.: A dynamical model for the study of tropical cyclone development, Geofisica Internacional (Mexico), 4, 187–198, 1964.

Rasmussen, E.: The polar low as an extratropical CISK disturbance, Quarterly Journal of the Royal Meteorological Society, 105, 531–549, 1979.

Rasmussen, E. A. and Turner, J.: Polar lows: Mesoscale Weather Systems in the Polar Regions, Cambridge University Press, 2003.

Reed, R. J.: Cyclogenesis in polar air streams, Monthly Weather Review, 107, 38–52, 1979.

Reed, R. J. and Blier, W.: A Case Study of Comma Cloud Development in the Eastern Pacific, Monthly Weather Review, 114, 1681–1695, 1986.

Reed, R. J. and Duncan, C. N.: Baroclinic instability as a mechanism for the serial development of polar lows: a case study, Tellus A, 39, 376–384, 1987.

Renfrew, I.: SYNOPTIC METEOROLOGY | Polar Lows, in: Encyclopedia of Atmospheric Sciences (Second Edition), edited by North, G. R., Pyle, J., and Zhang, F., pp. 379 – 385, Academic Press, Oxford, 2015.

Rojo, M., Claud, C., Mallet, P.-E., Noer, G., Carleton, A. M., and Vicomte, M.: Polar low tracks over the Nordic Seas: a 14-winter climatic analysis, Tellus A, 67, 2015.

Rojo, M., Claud, C., Noer, G., and Carleton, A. M.: In situ measurements of surface winds, waves, and sea state in polar lows over the North Atlantic, Journal of Geophysical Research: Atmospheres, 124, 700–718, 2019.

Rojo, M., Noer, G., and Claud, C.: Polar Low tracks in the Norwegian Sea and the Barents Sea from 1999 until 2019, PANGAEA, supplement to: Rojo et al. (2019), 2019.

Sardie, J. M. and Warner, T. T.: On the Mechanism for the, Development of Polar Lows, Journal of the Atmospheric Sciences, 40, 869–881, 1983.

Savitzky, A. and Golay, M. J.: Smoothing and differentiation of data by simplified least squares procedures., Analytical chemistry, 36, 1627–1639, 1964.

Shapiro, M. A. and Keyser, D.: Fronts, jet streams and the tropopause, in: Extratropical cyclones, pp. 167–191, Springer, 1990.

Smirnova, J. E. and Golubkin, P. A.: Comparing polar lows in atmospheric reanalyses: Arctic System Reanalysis versus ERA-Interim, Monthly Weather Review, 145, 2375–2383, 2017.

Stoelinga, M. T.: A potential vorticity-based study of the role of diabatic heating and friction in a numerically simulated baroclinic cyclone, Monthly weather review, 124, 849–874, 1996.

Stoll, P. J., Graversen, R. G., Noer, G., and Hodges, K.: An objective global climatology of polar lows based on reanalysis data, Quarterly Journal of the Royal Meteorological Society, 144, 2099–2117, 2018.

Stoll, P. J., Valkonen, T. M., Graversen, R. G., and Noer, G.: A well-observed polar low analysed with a regional and a global weather-prediction model, Quarterly Journal of the Royal Meteorological Society, 146, 1740–1767, 2020.

Terpstra, A., Spengler, T., and Moore, R. W.: Idealised simulations of polar low development in an Arctic moist-baroclinic environment, Quarterly Journal of the Royal Meteorological Society, 141, 1987–1996, 2015.

Terpstra, A., Michel, C., and Spengler, T.: Forward and reverse shear environments during polar low genesis over the North East Atlantic, Monthly Weather Review, 144, 1341–1354, 2016.

Vallis, G. K.: Atmospheric and oceanic fluid dynamics, Cambridge University Press, 2017.

Watanabe, S.-i. I., Niino, H., and Yanase, W.: Climatology of polar mesocyclones over the Sea of Japan using a new objective tracking method, Monthly Weather Review, 144, 2503–2515, 2016.

Wehrens, R., Buydens, L. M., et al.: Self-and super-organizing maps in R: the Kohonen package, Journal of Statistical Software, 21, 1–19, 2007.

Yanase, W. and Niino, H.: Dependence of polar low development on baroclinicity and physical processes: An idealized high-resolution numerical experiment, Journal of the Atmospheric Sciences, 64, 3044–3067, 2007.

Yanase, W., Fu, G., Niino, H., and Kato, T.: A polar low over the Japan Sea on 21 January 1997. Part II: A numerical study, Monthly Weather Review, 132, 1552–1574, 2004.

Zappa, G., Shaffrey, L., and Hodges, K.: Can polar lows be objectively identified and tracked in the ECMWF operational analysis and the ERA-Interim reanalysis?, Monthly Weather Review, 142, 2596–2608, 2014.